



Dedicated to innovation in aerospace

NLR-TP-2016-508 | November 2016

# Trajectory Planning and Trajectory Tracking for a Small-Scale Helicopter in Autorotation

CUSTOMER: Netherlands Aerospace Centre



NLR – Netherlands Aerospace Centre

## Netherlands Aerospace Centre

NLR is a leading international research centre for aerospace. Bolstered by its multidisciplinary expertise and unrivalled research facilities, NLR provides innovative and integral solutions for the complex challenges in the aerospace sector.

NLR's activities span the full spectrum of Research Development Test & Evaluation (RDT & E). Given NLR's specialist knowledge and facilities, companies turn to NLR for validation, verification, qualification, simulation and evaluation. NLR thereby bridges the gap between research and practical applications, while working for both government and industry at home and abroad.

NLR stands for practical and innovative solutions, technical expertise and a long-term design vision. This allows NLR's cutting edge technology to find its way into successful aerospace programs of OEMs, including Airbus, Embraer and Pilatus. NLR contributes to (military) programs, such as ESA's IXV re-entry vehicle, the F-35, the Apache helicopter, and European programs, including SESAR and Clean Sky 2.

Founded in 1919, and employing some 650 people, NLR achieved a turnover of 73 million euros in 2014, of which three-quarters derived from contract research, and the remaining from government funds.

For more information visit: [www.nlr.nl](http://www.nlr.nl)

# Trajectory Planning and Trajectory Tracking for a Small-Scale Helicopter in Autorotation



## Problem area

Helicopter power-off flight, or autorotation, is a condition in which no engine torque is applied to the Main Rotor (MR) and Tail Rotor (TR). This may happen in case of an engine failure, resulting in a flight condition which is somewhat comparable to gliding for a fixed-wing aircraft. During an autorotation, the MR is not driven by a running engine, but by air flowing through the rotor disk bottom-up, while the helicopter is descending.

The design of a high-performance guidance and control system for a small-scale helicopter Unmanned Aerial Vehicle (UAV), with an engine OFF flight condition (i.e. autorotation), is known to be a challenging task. Hence, it is the purpose of this paper to describe such a flight control system that enables a small-scale unmanned helicopter to execute a completely automatic landing maneuver, for an engine OFF flight condition.

## REPORT NUMBER

NLR-TP-2016-508

## AUTHOR(S)

S. Taamallah

X. Bombois

P.M.J. Van den Hof

## REPORT CLASSIFICATION

UNCLASSIFIED

## DATE

November 2016

## KNOWLEDGE AREA(S)

Aircraft Systems

Engineering

Helicopter Technology

## DESCRIPTOR(S)

Small-scale helicopter

autorotation

Robust control

Differential flatness

Unmanned aerial vehicle

## Description of work

The presented flight control solution incorporates a classic guidance and control logic, in which the guidance module is decoupled from the control module. The goal of the guidance module, or Trajectory Planning, is to generate open-loop, feasible and optimal autorotative trajectories, for the helicopter, whereas the aim of the control module, or Trajectory Tracking, consists in enabling the helicopter to fly along these optimal trajectories.

## Results and conclusions

The first real-time feasible, model-based Trajectory Planning and model-based Trajectory Tracking, for a small-scale helicopter in autorotation is being demonstrated using a high-fidelity, high-order, nonlinear helicopter simulation.

## Applicability

This paper demonstrates a model-based automatic safety recovery system that could safely fly and land a small-scale helicopter UAV in un-powered flight (i.e. autorotation).

### GENERAL NOTE

This report is based on a paper published in *Control Engineering Practice* (Vol. 58), January 2017, by Elsevier.

### NLR

Anthony Fokkerweg 2

1059 CM Amsterdam

p ) +31 88 511 3113 f ) +31 88 511 3210

e ) [info@nlr.nl](mailto:info@nlr.nl) i ) [www.nlr.nl](http://www.nlr.nl)



Dedicated to innovation in aerospace

NLR-TP-2016-508 | November 2016

# Trajectory Planning and Trajectory Tracking for a Small-Scale Helicopter in Autorotation

CUSTOMER: Netherlands Aerospace Centre

**AUTHOR(S):**

**S. Taamallah**

**X. Bombois**

**P.M.J. Van den Hof**

Netherlands Aerospace Centre




Ecole Centrale de Lyon

Eindhoven University of Technology

*This report is based on a paper published in Control Engineering Practice (Vol. 58), January 2017, by Elsevier.*

*The contents of this report may be cited on condition that full credit is given to NLR and the author(s).*

<b>CUSTOMER</b>	Netherlands Aerospace Centre
<b>CONTRACT NUMBER</b>	----
<b>OWNER</b>	NLR
<b>DIVISION NLR</b>	Aerospace Systems
<b>DISTRIBUTION</b>	Unlimited
<b>CLASSIFICATION OF TITLE</b>	UNCLASSIFIED

APPROVED BY :																				
AUTHOR				REVIEWER				MANAGING DEPARTMENT												
S. Taamallah 																				
DATE	2	6	1	0	1	6	DATE	2	6	1	0	1	6	DATE	2	6	1	0	1	6

# Contents

## Abstract

<b>1</b>	<b>Introduction</b>	
1.1	Main Contribution	2
1.2	Paper outline	4
<b>2</b>	<b>General control architecture</b>	<b>4</b>
<b>3</b>	<b>The helicopter High-Order Model (HOM)</b>	<b>5</b>
3.1	Modeling assumptions	6
3.1..1	Main rotor	6
3.1..2	Tail rotor	7
3.1..3	Fuselage	8
3.2	The dynamics of the nonlinear HOM	8
<b>4</b>	<b>Flatness-based Trajectory Planning (TP)</b>	<b>10</b>
4.1	Flat outputs	12
4.2	Flat output parametrization	12
4.3	Optimal trajectory planning for the engine OFF case (i.e. autorotation)	13
4.3.1	Cost functional	15
4.3.2	Final-time boundary condition	16
4.3..3	Trajectory constraints	17
<b>5</b>	<b>Robust control based Trajectory Tracking (TT)</b>	<b>17</b>
5.1	Linear multivariable $\mu$ control design	19
<b>6</b>	<b>Design of the engine OFF inner-loop controller</b>	<b>21</b>
6.1	Choice of nominal plant model for the inner-loop control design	22
6.2	Selection of weights	22
6.3	Controller synthesis and analysis	25
<b>7</b>	<b>Design of the engine OFF outer-loop controller</b>	<b>27</b>
7.1	Choice of nominal plant model for the outer-loop control design	27
7.2	Selection of weights	27
7.3	Controller synthesis and analysis	29
7.4	Adapting the engine OFF outer-lop controller	29
<b>8</b>	<b>Simulations results</b>	<b>30</b>
8.1	Setting up the trajectory planning for the engine OFF cases	30
8.2	Discussion of closed-loop simulation results	34
<b>9</b>	<b>Conclusion</b>	<b>39</b>

<b>Appendix A: nomenclature</b>	<b>41</b>
<b>References</b>	<b>43</b>



# Trajectory Planning and Trajectory Tracking for a Small-Scale Helicopter in Autorotation

Skander Taamallah<sup>a,\*</sup>, Xavier Bombois<sup>b</sup>, Paul M. J. Van den Hof<sup>c</sup>

<sup>a</sup>National Aerospace Laboratory (NLR), Anthony Fokkerweg 2, 1059 CM, Amsterdam, The Netherlands

<sup>b</sup>Laboratoire Ampère, UMR CNRS 5005, Ecole Centrale de Lyon, 36 avenue Guy de Collongue, 69134 Ecully Cedex, France

<sup>c</sup>Department of Electrical Engineering, Eindhoven University of Technology, Den Dolech 2, 5612 AZ, Eindhoven, The Netherlands

---

## Abstract

The design of a high-performance guidance and control system for a small-scale helicopter Unmanned Aerial Vehicles (UAV), with an engine OFF flight condition (i.e. autorotation), is known to be a challenging task. It is the purpose of this paper to present a Trajectory Planning (TP) and Trajectory Tracking (TT) system, having on-line computational tractability. The presented Flight Control System (FCS) is anchored within the aggregated paradigms of differential flatness based optimal planning, and robust control based tracking. In particular the first real-time feasible, model-based TP and model-based TT, for a small-scale helicopter in autorotation is being demonstrated using a high-fidelity, high-order, nonlinear helicopter simulation.

*Keywords:* Differential flatness, robust control, small-scale helicopter autorotation, unmanned aerial vehicle.

---

## 1. Introduction

Helicopter power-off flight, or autorotation, is a condition in which no engine torque is applied to the Main Rotor (MR) and Tail Rotor (TR). This may happen in case of an engine failure, resulting in a flight condition which is somewhat comparable to gliding for a fixed-wing aircraft. During an autorotation, the MR is not driven by

---

\*Corresponding author

Email addresses: [staamall@nlr.nl](mailto:staamall@nlr.nl) (Skander Taamallah), [xavier.bombois@ec-lyon.fr](mailto:xavier.bombois@ec-lyon.fr) (Xavier Bombois), [P.M.J.vandenhof@tue.nl](mailto:P.M.J.vandenhof@tue.nl) (Paul M. J. Van den Hof)

a running engine, but by air flowing through the rotor disk bottom-up, while the helicopter is descending [1, 2]. In this case, the power required to keep the rotor spinning is obtained from the vehicle's potential and kinetic energies. In addition, helicopters involve under-actuated, Multiple-Input Multiple-Output (MIMO), nonlinear, and unstable dynamics. When compared to full-size helicopters or even to larger helicopter Unmanned Aerial Vehicle (UAVs) (i.e. 100–200 kg), small-scale helicopters (i.e. under 10–20 kg) feature an increased power-to-mass ratio, have a very stiff main rotor assembly, and can produce much higher torque-to-inertia ratios. Small-scale helicopter UAVs are thus much more agile, and have higher levels of dynamics coupling and instability, when compared to larger size ones. Hence, the design of a guidance and control system, for a small-scale helicopter UAV in autorotation, becomes a challenging problem.

The purpose of this paper is to describe a, model-based, guidance and control logic that enables a small-scale unmanned helicopter to execute a completely automatic landing maneuver, for an engine OFF flight condition (i.e. autorotation). The guidance module, or Trajectory Planning (TP), shall be capable of generating optimal trajectories, on-line, subject to system constraints. On the other hand the control module, or Trajectory Tracking (TT), shall have the duty to ensure that the helicopter flies along these optimal trajectories. Finally, the complete Flight Control System (FCS) shall be evaluated on a three-dimensional (3D), high-fidelity, high-order, nonlinear helicopter simulation, developed in [3].

### *1.1. Main Contribution*

Very few papers, i.e. [4, 5, 6, 7], have addressed the aggregated planning and tracking functionalities, for the engine OFF case, with validation through either experiments or 3D high-fidelity nonlinear simulations. The authors in [6, 7] apply their FCS to the case of a full-size helicopter, whereas the application in [5] involves a so-called short-range/tactical size helicopter UAV (approximately 200 kg). Only the results in [4] are for a small-scale helicopter UAV.

Now the solution to the autorotation TP problem has traditionally been addressed within the off-line, computationally intensive, nonlinear optimal control framework

[8, 9, 10, 11, 12, 13, 14]. In our paper however, the selection of the TP is based upon a computationally tractable approach, i.e. the concept of differential flatness [15]. This approach allows us to exploit the rigid-body nonlinear dynamics, while retaining a high computational efficiency, e.g. for on-line use in a hard real-time environment where stringent timing constraints may need to be met (especially for high-bandwidth systems). In addition since the results in [4, 5, 6, 7] are based upon a model-free TP, our model-based planning shall generate trajectories which are both feasible and optimal.

Next, since the helicopter dynamics is nonlinear, the design of the TT controller shall necessitate an approach that effectively tries to exploit the system's nonlinear structure. For the case of TT for a helicopter with the engine ON, a vast array of technical avenues have been investigated over the years, with the application of: classical control [16], gain-scheduling of Proportional-Integral-Derivative (PID) controllers [17], Linear Quadratic Regulator (LQR) [18, 19], Linear Quadratic Gaussian (LQG) [20, 19], Linear Parameter-Varying (LPV) [21],  $H_2$  [22],  $H_\infty$  [23, 22, 24, 25],  $\mu$  [26, 21], (nonlinear) Model Predictive Control (MPC) [27, 28, 19], feedback linearization and Nonlinear Dynamic Inversion (NDI) [29, 30, 31], adaptive control [32, 33, 34, 35], and model-based learning approaches [36, 37, 38].

For the case of TT with the engine OFF, the method in [7] is based upon a model-free fuzzy logic approach. The method in [4] uses a model-based Differential Dynamic Programming (DDP) approach. The method in [6] uses a model-based combined NDI with PID loops, whereas the method in [5] uses a model-based  $H_\infty$  approach. For the three model-based approaches, the TT controllers are synthesized on a single nominal model, that does not include uncertainties. In our paper the choice is made for an approach that combines both simplicity and computational tractability, namely a robust control  $\mu$  strategy. The selected strategy consists in using a single, nominal, low-order, Linear Time-Invariant (LTI) plant, coupled with an input multiplicative uncertainty. This uncertainty is added here to compensate for the unmodeled plant nonlinearities

and unmodeled higher-order rotor dynamics<sup>1</sup>. By applying a small gain approach [39, 40], the robust controller synthesis consists in obtaining a controller insensitive to this multiplicative uncertainty at the plant input.

Summing up, we present in this paper the first real-time feasible, model-based TP and TT system, for the case of a small-scale helicopter UAV in autorotation.

### 1.2. Paper Outline

The remainder of this paper is organized as follows. In Section 2, the two-stage control architecture is first recalled. In Section 3, the high-order helicopter nonlinear model, used to validate the FCS, is briefly reviewed. In Section 4, the flatness-based trajectory planning is described. In Section 5, the main aspects of the robust control approach are reviewed and discussed. In Section 6 and Section 7, the synthesis of the inner- and outer-loop controllers are presented. In Section 8, simulation results are analyzed. Finally, conclusions and future directions are presented in Section 9.

## 2. General control architecture

The conceptual FCS design solution, chosen to solve the helicopter UAV guidance and control problem, is here presented. The classical two-stage controller design paradigm is being used, in which the philosophy decouples the guidance module from the control module. The guidance module, or TP, shall be capable of generating open-loop, feasible and optimal (autorotative) trajectory references  $\mathbf{x}_{\text{TP}}$ , for the small-scale helicopter, subject to system and environmental constraints, see Fig. 1. This TP computes open-loop optimal trajectories, given a cost objective, system dynamics, and controls and states equality and inequality constraints. These trajectories may be computed off-line, through the use of nonlinear optimal control methods, or alternatively such as in this paper, may be computed on-line using the concept of differential flatness.

On the other hand the control module, or TT, shall compare the current measured values  $\mathbf{y}$ , i.e. a subset of the vehicle states  $\mathbf{x}$ , with the reference values  $\mathbf{x}_{\text{TP}}$  produced by the

---

<sup>1</sup>Unmodeled in the low-order nominal LTI plant used for control design, these are however modeled in the high-order nonlinear helicopter model.

TP, and shall formulate the feedback controls  $\mathbf{u}$  aimed at decreasing this tracking error<sup>2</sup>. This latter may be due to a combination of model uncertainty (unmodeled higher-order dynamics, unmodeled static nonlinearities, parametric uncertainties, delays), and signal uncertainty (wind disturbances and noise). In Fig. 1, the Helicopter Dynamics NonLinear Simulation block refers to the high-fidelity, nonlinear, High-Order Model (HOM), simulation, developed in [3], serving as a proxy for the real helicopter system.

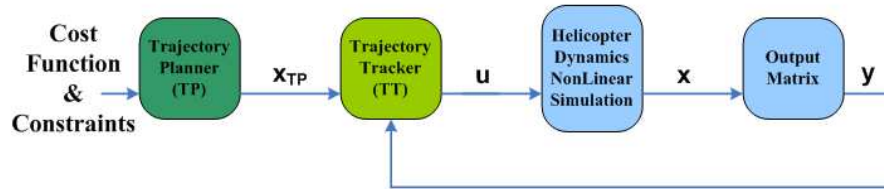


Figure 1: Two-stage control architecture

### 3. The helicopter High-Order Model (HOM)

This Section briefly reviews the comprehensive HOM, used as a realistic small-scale helicopter simulation environment, for the validation of the FCS. This high-fidelity, MATLAB<sup>®</sup>-based model represents a white-box, nonlinear and continuous-time description of the helicopter flight dynamics. This model aims at simulating the helicopter flight dynamics for the case of a flybarless<sup>3</sup>, articulated, Pitch-Lag-Flap (P-L-F) MR with rigid blades, for both ClockWise (CW) or Counter-ClockWise (CCW) MR rotation. The model incorporates the rigid-body dynamics, MR dynamics, TR, fuselage, and tails.

<sup>2</sup>The nomenclature, given in Appendix A, states that all vectors are printed in boldface, hence the control input vector  $\mathbf{u}$  should not be confused with the body longitudinal velocity  $u$ .

<sup>3</sup>The flybar is a mechanical component of the helicopter's main rotor system, and consists of a rod carrying small aerofoils (paddles). A flybar on a main rotor enhances the stability of the helicopter and hence, for a pilot using a Remote-Control (RC) device, the flybar system makes the helicopter easier to fly. However, small-scale flybarless (i.e. without these stabilizing paddles) helicopters are becoming increasingly popular, since flybarless rotors allow for increased helicopter agility and performance, and reduced rotor mechanical complexity.

### 3.1. Modeling assumptions

We review first all assumptions made while deriving the nonlinear helicopter model, i.e. structural, aerodynamics, and dynamical simplifications. The presented assumptions are valid for stability and control investigations of helicopters up to an advance ratio limit of about 0.3 [41, 42, 43].

#### 3.1.1. Main rotor

##### **Structural simplifications**

- Rotor shaft forward and lateral tilt-angles are zero. Rotor precone is also zero. The blade has zero twist, constant chord, zero sweep, constant thickness ratio, and a uniform mass distribution.
- We assume a rigid rotor blade in bending. We neglect higher modes (harmonics), since higher modes are only pronounced at high speed [44, 45]. Blade torsion is neglected since small-scale helicopter blades are generally relatively stiff.
- Rotor inertia inboard of the flap hinge is also neglected.

##### **Aerodynamics simplifications**

- Main rotor inflow is modeled as the three-states Pitt-Peters model [46, 47], with a correction for flight into the Vortex-Ring-State (VRS)<sup>4</sup> from [48].
- Vehicle flies at a low altitude, hence neglecting air density and temperature variations. Blade element theory is used to compute rotor lift and drag forces. Radial flow along blade span is ignored. Pitch, lag, and flap angles are assumed to be small.
- Compressibility effects are disregarded, which is a reasonable assumption considering small-scale helicopter flight characteristics. Viscous flow effects are also disregarded, which is a valid assumption for low Angle Of Attack (AOA) and un-separated flow [49, 50].

---

<sup>4</sup>Briefly summarized, the VRS corresponds to a condition where the helicopter is descending in its own wake, resulting in a chaotic and dangerous flight condition [1].

- Aerodynamic interference effects between the main rotor and other helicopter modules, e.g. fuselage or tail rotor, are neglected.
- The presence of the fuselage just under the main rotor acts as a so-called pseudo-ground effect [51], resulting in some thrust recovery. This phenomenon is also neglected.
- Wake bending during maneuvering flight is neglected.

#### **Dynamical simplifications**

- Dynamic twist is neglected. Hence blade Center of Gravity (CG) is assumed to be colocated with blade section quarter chord line.
- Unsteady (frequency dependent) effects for time-dependent development of blade lift and pitching moment, due to changes in local incidence, are ignored; e.g. dynamic stall, due to rapid pitch changes, is ignored.

#### *3.1.2. Tail rotor*

##### **Structural simplifications**

- The blade has zero twist, constant chord, zero sweep, and has constant thickness ratio. The blade is also rigid, hence torsion is neglected.

##### **Aerodynamics simplifications**

- Linear lift with constant lift curve slope, and uniform induced flow over the rotor are assumed.
- Aerodynamic interference effects from the main rotor is neglected. Similarly, the interference from the vertical tail (due to blockage) is also neglected.
- Compressibility, blade stall, and viscous flow effects are also disregarded.

##### **Dynamical simplifications**

- Blade dynamics is disregarded. Unsteady effects are neglected.

### 3.1.3. Fuselage

#### **Aerodynamics simplifications**

- Fuselage aerodynamic center is collocated with vehicle CG. Further, only steady airloads effects are considered.
- Effect of rotor downwash on fuselage is neglected.

### 3.2. The dynamics of the nonlinear HOM

From Fig. 1, and zooming on the 'Helicopter Dynamics Nonlinear Simulation' block, one obtains Fig. 2 which gives additional insight into the model. The control input-vector  $\mathbf{u}$  is of dimension four, and the state-vector  $\mathbf{x}$  of dimension twenty-four. The states include the twelve-states rigid-body motion (states given in blue), and the dynamics of the MR (states given in red). The former includes the three-states inertial position, the three-states body linear velocities, the three-states body rotational velocities, and the three-states attitude (orientation) angles, see Fig. 2. The dynamics of the MR include the helicopter higher frequency phenomena, which exist for both the engine ON and OFF (i.e. autorotation) flight conditions. These include the MR three-states dynamic inflow [47, 52], with a correction for flight in the VRS [48], and MR blade flap-lag dynamics with each blade being defined by its, four-states, flap/lag angles and rotational velocities [53], see Fig. 2. Regarding the MR Revolutions Per Minute (RPM), it is generally assumed fixed for the engine ON case, whereas for the engine OFF case it is not fixed anymore. Indeed, the MR RPM represents an essential part of the autorotative flight condition, and this additional state needs to be included in the state-vector  $\mathbf{x}$  when considering the engine OFF case, see Fig. 2. Other model components include: 1) the TR, modeled as a standard Bailey type rotor [54]; 2) the fuselage based upon aerodynamic lift and drag coefficients which are tabulated as a function of airflow AOA and sideslip angles<sup>5</sup>; and 3) the Horizontal and Vertical Tails

---

<sup>5</sup>These aerodynamic lookup tables have been obtained by scaling-down a full-size Bo-105 helicopter fuselage aerodynamic model.





Figure 2: Helicopter Inputs  $\mathbf{u}$  (in green), States  $\mathbf{x}$  (in blue the rigid-body states, in red the main rotor states), and Measurements  $\mathbf{y}$  (measured states)

(HT and VT), based upon standard flat plate models. Next, there is the vector of measured outputs  $\mathbf{y}$  of dimension twelve. The measurements are given by  $\mathbf{y} = \mathbf{x}_{(1:12)}$ , with  $\mathbf{x}_{(1:12)}$  a shorthand for the first twelve states of  $\mathbf{x}$ , i.e. the rigid-body states (see also the nomenclature in Appendix A). Thanks to the modeling assumptions made in Section 3.1, the helicopter flight dynamics model can be expressed as a set of first-order, Ordinary Differential Equations (ODEs), rather than the more complex Partial Differ-

ential Equations (PDEs) formulations, such that

$$\forall t \geq 0 \quad \dot{\mathbf{x}}(t) = f(\mathbf{x}(t), \mathbf{u}(t)) \quad (1)$$

with  $f(\cdot)$  a continuous-time function. This helicopter HOM has shown to be in good agreement with an equivalent FLIGHTLAB<sup>6</sup> model, for both static (trim) and dynamic conditions, see [56, 3]. This HOM will be used for the validation of the FCS, but due to its complexity, approximation of this HOM will be used for controller design.

#### 4. Flatness-based Trajectory Planning (TP)

The seminal ideas of differential flatness were introduced in the early 1990s in [15, 57] in which certain differential algebraic representations of dynamical systems are equivalent. Flatness allows for a complete parametrization of all system variables—inputs, states, and outputs—in terms of a finite set of independent variables, called flat outputs, and a finite number of their derivatives [58, 59]. Flat parameterizations result in optimization problems with fewer variables [60], i.e. by the complete elimination of the dynamical constraints. In this case, a trajectory generation problem is transformed from a dynamic to an algebraic one, in which the flat outputs are parametrized over a space of basis functions, for which the generation of feasible trajectories is reduced to a classical algebraic interpolation or collocation problem [61, 62]. This allows, in principle, for significant computational benefits. With regard to applications, it was shown that simplified dynamics of aircraft and Vertical Take-Off and Landing (VTOL) aircraft are flat [63, 64, 65, 66, 67], simplified helicopter dynamics is flat [68, 69, 58], and simplified quadrotor dynamics is flat [70, 71, 72, 73], whereas more realistic vehicle models are in general non-differentially flat, e.g. [58].

Since high-fidelity helicopter models are known to be non-differentially flat, a standard approach in the literature, to circumvent this difficulty, has consisted in progressively simplifying these models until they become flat. The drawback is that the do-

---

<sup>6</sup>FLIGHTLAB is a state of the art modeling, analysis and real-time simulation tool, used world-wide to simulate helicopter flight dynamics [55].

main of validity, of these simplified representations, becomes questionable. Hence, rather than generating optimal trajectories based upon such questionable models, an alternative approach is here chosen, consisting in using only the rigid-body dynamics as the model for the TP, with total aerodynamic forces and total moments as the plant inputs (rather than the vehicle control inputs). Obviously, this corresponds also to a simplification of the helicopter HOM (discussed in Section 3), since the HOM is being replaced by the low-order rigid-body dynamics. However, if the bandwidth of the control inputs is kept low, replacing the helicopter HOM with only the rigid-body dynamics becomes acceptable for planning purposes. The main drawback of using the rigid-body dynamics, as a substitute for the helicopter HOM, comes from losing the relationship between the total aerodynamic forces/moments and the vehicle control inputs. In our case, this should not represent a major liability since, as hinted upon in Section 2, the TP module does not feedforward the control inputs. On the other hand, the advantage of using the rigid-body dynamics (as the TP model) is that it can be shown to be exactly flat. The ideas of differential flatness in conceptual form are recalled next [15, 57]. First it is supposed that a plant's nonlinear model, derived from first-principles, is available and given by

$$\forall t \geq 0 \quad \dot{\mathbf{x}}(t) = \tilde{f}(\mathbf{x}(t), \mathbf{u}(t)) \quad (2)$$

with  $\tilde{f}(\cdot)$  a continuous-time, partially differentiable (sufficiently) smooth function, with  $\mathbf{x}(t) \in \mathcal{P}_x \subset \mathbb{R}^{n_x}$  the plant state,  $\mathbf{u}(t) \in \mathcal{P}_u \subset \mathbb{R}^{n_u}$  the control input,  $t$  the time variable, and  $(\mathcal{P}_x, \mathcal{P}_u)$  some compact sets. Next the following definition from [59] is given.

**Definition 1.** *The system given by Eq. (2) is differentially flat if there exists a flat output  $\mathbf{z}(t) \in \mathcal{P}_z \subset \mathbb{R}^{n_z}$ ,  $n_z = n_u$ , two integers  $r$  and  $s$ , a mapping  $\psi(\cdot) : \mathbb{R}^{n_x} \times (\mathbb{R}^{n_u})^{s+1} \rightarrow \mathbb{R}^{n_u}$  of rank  $n_u$ , a mapping  $\phi_0(\cdot) : (\mathbb{R}^{n_u})^{r+1} \rightarrow \mathbb{R}^{n_x}$  of rank  $n_x$ , and a mapping  $\phi_1(\cdot) : (\mathbb{R}^{n_u})^{r+2} \rightarrow \mathbb{R}^{n_u}$  of rank  $n_u$ , with all mappings in a suitably chosen open subset, such that*

$$\begin{aligned} \mathbf{z}(t) &:= \psi(\mathbf{x}(t), \mathbf{u}(t), \dot{\mathbf{u}}(t), \dots, \mathbf{u}^{(s)}(t)) \\ \mathbf{x}(t) &:= \phi_0(\mathbf{z}(t), \dot{\mathbf{z}}(t), \dots, \mathbf{z}^{(r)}(t)) \\ \mathbf{u}(t) &:= \phi_1(\mathbf{z}(t), \dot{\mathbf{z}}(t), \dots, \mathbf{z}^{(r+1)}(t)) \end{aligned} \quad (3)$$

**Remark 1.** *If such mappings can be found then the differential equation  $\frac{d}{dt}\phi_0(\cdot) = f(\phi_0(\cdot), \phi_1(\cdot))$  is identically satisfied [59].*

**Remark 2.** *In some cases,  $\mathbf{z}$  is in fact a subset of the state-vector  $\mathbf{x}$ . The function  $\psi(\cdot)$  is then obvious.*

Now, simplified aircraft dynamics was shown to be flat in [63], whereas simplified helicopter dynamics was also shown to be flat in [69]. In the sequel, we briefly recall that the rigid-body dynamics, in the body-axis frame (as given in Appendix C of Chapter 2 in [56]), is flat when choosing the following six specific states as flat outputs.

#### 4.1. Flat outputs

Recall that the twelve rigid-body states have been defined in Fig. 2 of Section 3

$$\mathbf{x} = \begin{pmatrix} x_N & x_E & x_Z & u & v & w & p & q & r & \phi & \theta & \psi \end{pmatrix}^T \quad (4)$$

**Lemma 1.** *Let real scalars  $n_x$  and  $n_u$ , of Definition 1, be chosen such that  $n_x = 12$  and  $n_u = 6$ . By selecting the following six body states as flat outputs*

$$\mathbf{z} = \begin{pmatrix} x_N & x_E & x_Z & \phi & \theta & \psi \end{pmatrix}^T \quad (5)$$

*Then the remaining six body states*

$$\begin{pmatrix} u & v & w & p & q & r \end{pmatrix}^T \quad (6)$$

*and the forces inputs  $\mathbf{F}_{CG}^b = (F_{CGx}^b F_{CGy}^b F_{CGz}^b)^T$  and moments inputs  $\mathbf{M}_{CG}^b = (M_{CGx}^b M_{CGy}^b M_{CGz}^b)^T$  can be expressed in terms of the flat outputs  $\mathbf{z}$  and their derivatives.*

**Proof 1.** *See Appendix E of Chapter 4 in [56].*

#### 4.2. Flat output parametrization

To transform the trajectory planning problem from an infinite-dimensional one to a finite one, a parametrization of the flat outputs  $\mathbf{z} = \begin{pmatrix} x_N & x_E & x_Z & \phi & \theta & \psi \end{pmatrix}^T$  over a space of basis functions is required. Here numerous alternatives are available,

e.g. generic polynomial parameterizations have been addressed in [58, 74, 59], spline parameterizations have been applied in [75, 76, 77], whereas pseudospectral parameterizations have been used in [78, 79]. In this paper, and with a view on using a computationally tractable approach, elementary polynomial parameterizations are called upon, as was also done in [58, 59]. Using Eq. (5), the flat outputs can be expressed as

$$\mathbf{z}(t) = \begin{pmatrix} x_N(t) & x_E(t) & x_Z(t) & \phi(t) & \theta(t) & \psi(t) \end{pmatrix}^\top = \left( \sum_{i=0}^n a_{i,1} t^i \dots \sum_{i=0}^n a_{i,n_u} t^i \right)^\top \quad (7)$$

with  $t$  the time variable, and  $\{a_{i,j}\}_{(i=0,j=1)}^{(i=n,j=n_u)}$  the to-be-determined polynomial coefficients. From this flat output definition, and from the rigid-body dynamics, it is inferred that integer  $r = 1$  in Definition 1. Now, from [59] one needs to choose  $n$  such that  $n \geq 2(r+1) + 1 \Rightarrow n \geq 5$ . In order to increase the likelihood of finding feasible trajectories, especially for the autorotation case, the integer  $n$  should be chosen much higher than its lower bound, i.e.  $n \gg 5$ . However, choosing a high  $n$  will inevitably increase the computational cost of the optimization problem, hence a trade-off needs to be considered. Based upon simulation results, a value of  $n = 7$  is chosen as this provides a good compromise between trajectory smoothness and computational cost.

#### 4.3. Optimal trajectory planning for the engine OFF case (i.e. autorotation)

The TP optimization problem consists of a cost functional  $J(\cdot)$ , with contributions from a fixed cost  $\Phi(\cdot)$ , and a running cost over time  $\int_{\Omega} \Psi(\cdot) dt$ , with the independent time variable  $t$  defined over the time domain  $\Omega = (T_o, T_f)$ , where the final time  $T_f$  may be free or fixed. This cost is given by

$$J(\mathbf{x}(t), \mathbf{u}(t), T_o, T_f) := \Phi(\mathbf{x}(T_o), \mathbf{x}(T_f), T_f) + \int_{\Omega} \Psi(\mathbf{x}(t), \mathbf{u}(t), t) dt \quad (8)$$

From Definition 1, this cost is equivalently expressed as a function of the flat output  $\mathbf{z}$

$$\begin{aligned} J(\phi_0(\mathbf{z}(t), \dot{\mathbf{z}}(t)), \phi_1(\mathbf{z}(t), \dot{\mathbf{z}}(t), \ddot{\mathbf{z}}(t)), T_o, T_f) &:= \Phi(\phi_0(\mathbf{z}(T_o), \dot{\mathbf{z}}(T_o)), \phi_0(\mathbf{z}(T_f), \dot{\mathbf{z}}(T_f)), T_f) \\ &+ \int_{\Omega} \Psi(\phi_0(\mathbf{z}(t), \dot{\mathbf{z}}(t)), \phi_1(\mathbf{z}(t), \dot{\mathbf{z}}(t), \ddot{\mathbf{z}}(t)), t) dt \end{aligned} \quad (9)$$

with the mappings  $\phi_0(\cdot)$  and  $\phi_1(\cdot)$ , derived from the rigid-body dynamics and given by Eq.(4.39)–Eq.(4.44) in [56]. The solution to the optimal trajectory planning gives the

optimal polynomial coefficients  $\{\hat{a}_{i,j}\}_{(i=0,j=1)}^{(i=n,j=n_u)}$  which minimize the cost functional  $J(\cdot)$

$$\{\hat{a}_{i,j}\}_{(i=0,j=1)}^{(i=n,j=n_u)} := \arg \min_{a_{i,j} \in \mathbb{R}} J(\phi_0(\mathbf{z}(t), \dot{\mathbf{z}}(t)), \phi_1(\mathbf{z}(t), \dot{\mathbf{z}}(t), \ddot{\mathbf{z}}(t)), T_o, T_f) \quad (10)$$

while enforcing the following constraints

- An initial-time boundary condition which corresponds, in our case, to the initial values of the control inputs  $\phi_1(\mathbf{z}(T_o), \dot{\mathbf{z}}(T_o), \ddot{\mathbf{z}}(T_o))$  and states  $\phi_0(\mathbf{z}(T_o), \dot{\mathbf{z}}(T_o))$ .
- A final-time boundary inequality condition, of the form

$$B_f(\phi_0(\mathbf{z}(T_f), \dot{\mathbf{z}}(T_f)), \phi_1(\mathbf{z}(T_f), \dot{\mathbf{z}}(T_f), \ddot{\mathbf{z}}(T_f)), T_f) \leq 0 \quad (11)$$

- An algebraic trajectory inequality constraint, of the form

$$T(\phi_0(\mathbf{z}(t), \dot{\mathbf{z}}(t)), \phi_1(\mathbf{z}(t), \dot{\mathbf{z}}(t), \ddot{\mathbf{z}}(t))) \leq 0 \quad t \in \Omega \quad (12)$$

**Remark 3.** *There are here no first-order ODEs constraints that need to be enforced. This allows for significant computational benefits.*

Now, computing a numerical solution to the continuous-time problem formulation, Eq. (9)–Eq. (12), requires first some form of problem discretization. Again with an eye on computational tractability, a simple discretization scheme is chosen, involving  $K$  collocation points, evenly spaced on domain  $\Omega$  (i.e. resulting in the discretized domain  $\Omega_K = \{T_o \ t_1 \dots \ t_{K-2} \ T_f\}$ ). Here a simple rectangular discretization approach, with 16 evenly spaced points<sup>7</sup>, is used. Obviously better discretization methods exist, however our objective is also to keep the computational cost to a minimum. Once discretized, our problem is transcribed into a NonLinear Programming problem (NLP) [80, 81], this latter being solved numerically by well known and efficient optimization techniques. In our case the MATLAB function *fmincon* of the Optimization Toolbox is used, based upon an Interior Point (IP) method [82, 83, 84, 85]. This nonlinear

---

<sup>7</sup>Based upon simulation results with initial altitudes below 100 m, the choice of 16 collocation points provided a good compromise between accuracy and computational tractability. It is acknowledged that this is a rather empirical justification.

optimization takes a few seconds to complete in a MATLAB environment (and may likely be one or two orders of magnitude faster, once exported to C language and compiled on-board an embedded computer). Next, the various elements of our optimization problem in Eq. (9)–Eq. (12) are addressed in more details.

#### 4.3.1. Cost functional

First, the fixed cost  $\Phi(\cdot)$  is set to zero. Indeed, this fixed cost may equivalently be replaced by tight bounds on the final state values. In turn this simplifies the optimization process, and lowers the computational time. Next, the cost objective for the un-powered flight case, i.e. autorotation landing, is defined as a running cost over time, and is given by

$$\begin{aligned} J_{OFF}(\mathbf{x}(t), \mathbf{u}(t)) = & \int_{\Omega} \left[ (\dot{F}_{CGx}^b)^2 + (\dot{F}_{CGy}^b)^2 + (\dot{F}_{CGz}^b)^2 \right. \\ & + (\dot{M}_{CGx}^b)^2 + (\dot{M}_{CGy}^b)^2 + (\dot{M}_{CGz}^b)^2 \\ & \left. + W_u u^2 + W_v v^2 + W_w w^2 + W_{\psi} (\psi - \psi_f)^2 \right] dt \end{aligned} \quad (13)$$

The cost in Eq. (13) minimizes the rate of all forces and moments  $(\dot{F}_{CGx}^b)^2 + (\dot{F}_{CGy}^b)^2 + (\dot{F}_{CGz}^b)^2 + (\dot{M}_{CGx}^b)^2 + (\dot{M}_{CGy}^b)^2 + (\dot{M}_{CGz}^b)^2$ , and therefore encourages smoother control policies. This is because the true control inputs do not appear in the model of Section 4.1 (in this model the forces and moments are the inputs). The purpose here is to: 1) minimize the battery power consumption; and 2) avoid *bang-bang* type solutions, that might excite undesirable high frequency dynamics or resonances. The term  $u^2 + w^2$  is added to limit the excessive build-up of vehicle kinetic energy during the descent. In particular, a high kinetic energy complicates the flare maneuver, since more energy needs to be dissipated, i.e. the timing of the control inputs becomes increasingly critical [1]. The term  $v^2$  is added to limit vehicle sideslip flight. Large sideslip decreases the flight performance, by increasing vehicle drag, increasing roll/yaw coupling, and hence increasing the workload of any feedback TT controller. The term  $\psi_f$  refers to the wind heading angle (known through either on-board measurements, or data-uplink from a ground-based wind sensor), and the term  $(\psi - \psi_f)^2$  is added to encourage flight and landing into the wind. This results in better flight performance, and lowers the vehicle kinetic energy at touchdown. Finally, the additional weights, i.e.  $W_u$ ,  $W_v$ ,  $W_w$ , and  $W_{\psi}$ , have been added to allow for the evaluation of various trade-offs.

#### 4.3.2. Final-time boundary condition

With respect to the final-time boundary condition, as expressed in Eq. (11), the aim is here twofold: 1) set the vehicle on the ground, possibly at a specified location; and 2) provide tight bounds on the vehicle kinetic energy and attitude angles, in accordance with technical specifications for safe landing. Specifically the definition of a 'successful', i.e. safe, autorotation landing, is given next.

**Definition 2.** A successful autorotation landing is defined as follows

- Body horizontal velocities with final values such that  $|u| \leq 0.5$  m/s and  $|v| \leq 0.5$  m/s. Non-zero horizontal velocities allow for a so-called slide-on-skids landing.
- Body vertical velocity with a final value such that  $|w| \leq 0.25$  m/s.
- Roll and pitch angles with final values such that  $|\phi| \leq 10^\circ$  and  $|\theta| \leq 10^\circ$ .

*Bound on total flight time.* In [56], it was found that for a fixed initial height above ground, increasing the initial helicopter velocity had only a relatively limited effect on flight time and hence stabilized rate of descent. This potentially indicates that the flight time, in autorotation, is only lightly correlated with the initial vehicle velocity, whereas it is primarily influenced by the initial height above ground. This led us to consider an empirical bound  $T_{OFF}$  on flight time  $T_f$ , such that  $T_f \leq T_{OFF}$ , with  $T_{OFF}$  deduced from simulation experiments as follows: Let  $x_{Z_i}$  be the initial height above ground at the instant of engine failure, and recall  $v_{ih}$  to be the helicopter induced velocity in hover, then the bound  $T_{OFF}$  is set, after several simulation experiments<sup>8</sup>, within the range:

$$\frac{x_{Z_i}}{1.75v_{ih}} \leq T_{OFF} \leq \frac{x_{Z_i}}{1.50v_{ih}} \quad (14)$$

<sup>8</sup>The coefficients 1.50 and 1.75 in  $\frac{x_{Z_i}}{1.75v_{ih}} \leq T_{OFF} \leq \frac{x_{Z_i}}{1.50v_{ih}}$  are empirically deduced, after several simulation experiments, for the case of the small-scale Align T-REX helicopter, which is the vehicle used in all of our simulations. A different helicopter, or even an Align T-REX helicopter with a different main rotor inertia, may likely result in different coefficient values.



**Remark 4.** *The reason for bounding the flight time  $T_f \leq T_{OFF}$  is as follows. Although the main rotor RPM dynamics is used in the helicopter nonlinear HOM, the RPM dynamics is not included in the flat model description, i.e. in Section 4.1, since not part of the rigid-body dynamics. By so doing, the same flat model can be used for both the engine OFF and ON cases, hence simplifying the trajectory planning software. However, excluding the main rotor RPM dynamics from the planning problem is only possible, i.e. will result in feasible autorotative trajectories, if the trajectory flight time is kept small enough. Further, since the RPM dynamics is eliminated from the planning problem, the main rotor RPM  $\Omega_{MR}$  signal may not be required for the trajectory tracking system either. Thus, the standard requirement consisting of adding a dedicated magnetic or optical RPM sensor, on the main rotor shaft or on the gear-box of a small-scale helicopter, may here be dropped.*

#### 4.3.3. Trajectory constraints

Regarding the trajectory constraints, as expressed in Eq. (12), the aim is here four-fold: 1) account for the vehicle's inherent physical and flight envelope limitations (e.g. bounds on speeds and attitude angles); 2) account for environmental constraints (e.g. the helicopter cannot descend below ground); 3) check for forces/moments range limitations; and finally 4) avoid ground strike by the tail rotor blade tip, just before touchdown, see our work in [86].

## 5. Robust control based Trajectory Tracking (TT)

The TT should allow the vehicle to fly along previously planned optimal trajectories. However, with four control inputs—longitudinal, lateral, vertical, and yawing motion—and six degrees of freedom—position and orientation in 3D space—the helicopter has two under-actuated degrees of freedom, corresponding to the roll and pitch motion, which inevitably limit the performance of the tracking system. Control over position and velocity is a primary objective of our application, hence the helicopter shall track the following seven references, namely 3D inertial positions  $(x_N \ x_E \ x_Z)^T$ , 3D body velocities  $(u \ v \ w)^T$ , and heading angle  $\psi$ . In addition, based upon simulation results using the helicopter HOM, it is found that position dynamics is much slower

than velocity dynamics. This justifies a design philosophy based upon the successive loop closure of feedback loops, where a sequential design process of inner- and outer-loops is sought, sometimes referred as a *Master-Slave* control configuration see Fig. 3. This design approach is related to the well-known time-scale separation principle [87], between slow and fast dynamics of a dynamical system, and supposes that the bandwidth of the inner-loop is much higher than the bandwidth of the outer-loop.

The outer-loop aims at tracking the planned inertial 3D position  $(x_N \ x_E \ x_Z)_{TP}^T$ . On

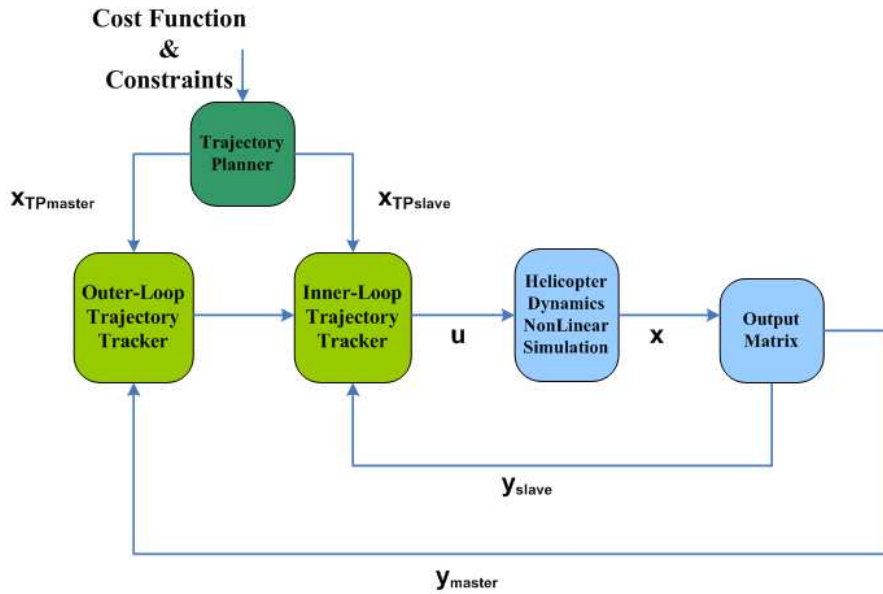


Figure 3: Master-Slave control configuration

the other hand, the role of the inner-loop consists in tracking the planned heading  $\psi_{TP}$ , and the planned 3D body linear velocities  $(u \ v \ w)_{TP}^T$ , these latter being adjusted by the outputs of the outer-loop controller  $(u \ v \ w)_d^T$  to allow for position control, see Fig. 4 and Fig. 5. In these figures,  $\mathbf{x}$  represents the state-vector (with dimension twenty-four), defining the states of the nonlinear helicopter HOM. The  $(u \ v \ w)_d^T$  can be seen as a "delta" correction to the nominal velocities  $(u \ v \ w)_{TP}^T$ . Hence, the to-be-tracked velocities by the inner-loop controller are given by  $(u \ v \ w)_{TP}^T + (u \ v \ w)_d^T$ . Next, since the outputs of the outer-loop are given in the inertial frame, a nonlinear inversion to convert the

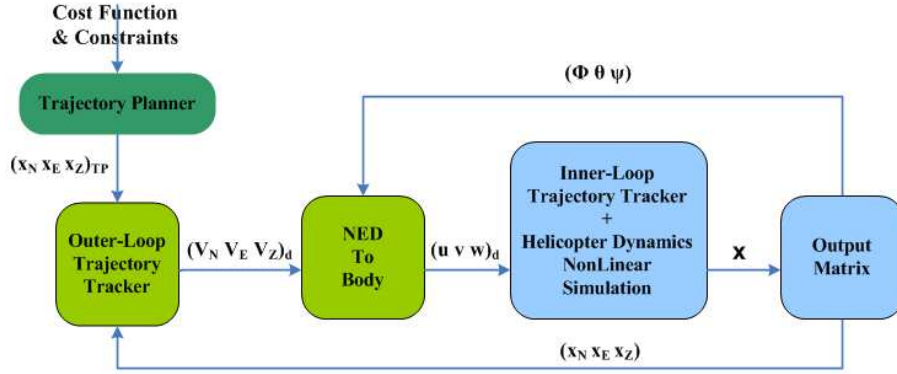


Figure 4: Outer-Loop, control interconnection diagram

reference velocities from NED to body frame is used, i.e.  $(u \ v \ w)_d^T = \mathbb{T}_{ob}^T (V_N \ V_E \ V_Z)_d^T$ , with the rotation matrix  $\mathbb{T}_{ob}$  given in Eq.(2.8) of Chapter 2 in [56]. Note also that in Fig. 5 all signals, except position, are fed-back into the controller to improve the closed-loop performance.

### 5.1. Linear multivariable $\mu$ control design

Both, the inner- and outer-loop controllers are designed according to the robust control design paradigm, in a two-degree of freedom control structure (i.e. using both feedback and feedforward). We have found that excluding modeling uncertainties from the inner and outer-loops tracking design process resulted in unsuccessful landings. Similarly, the two-degree of freedom structures also proved to be necessary both in the inner and outer loops since simpler structures led to poorer performance.

Note that the feedback part is used to reduce the effect of uncertainty, whereas the feed-forward part is added to improve tracking performance [88], and for optimality, both feedback and feedforward are designed in one step. First, a nominal plant  $P(s)$  (and  $P_d(s)$  for the disturbance) is obtained by linearizing the nonlinear helicopter model at some specified condition (to be discussed in the sequel). Next the generalized plant  $G_P(s)$  is defined, which maps the exogenous inputs  $\mathbf{w} = [\mathbf{n}^T \ \mathbf{r}^T \ \mathbf{d}^T]^T$  and control inputs  $\mathbf{u}$ , to controlled outputs  $\mathbf{z} = [\mathbf{z}_u^T \ \mathbf{z}_p^T]^T$  and measured outputs  $\mathbf{v} = [\mathbf{r}^T \ \mathbf{y}^T]^T$ , see Fig. 6. The signals include also the sensors noise  $\mathbf{n}$  (and  $\mathbf{n}_o$ ), the reference signals  $\mathbf{r}$ ,

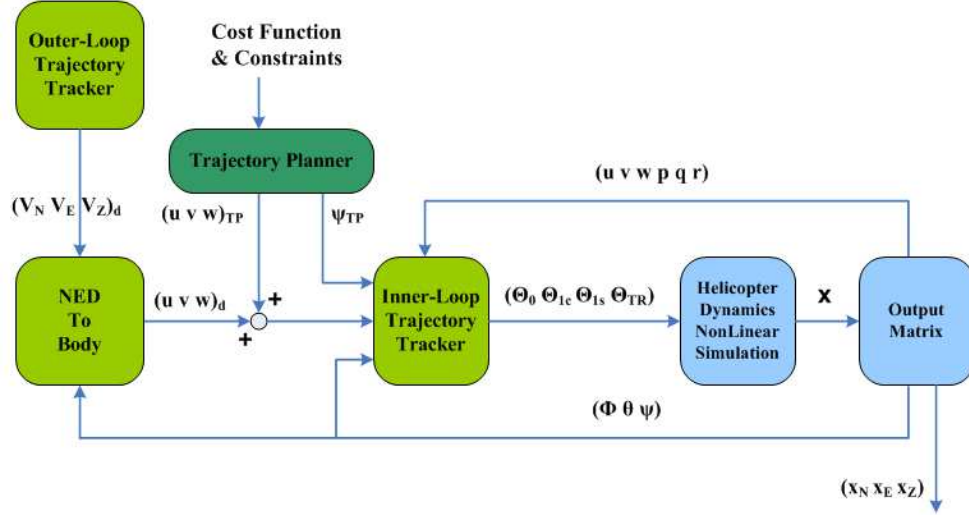


Figure 5: Inner-Loop, control interconnection diagram

the disturbance signals  $\mathbf{d}$ , the actuators performance signal (to limit actuator deflection magnitudes and rates)  $\mathbf{z}_u$ , the desired performance in terms of closed-loop signal responses  $\mathbf{z}_p$ , and the system outputs  $\mathbf{y}$  (and  $\mathbf{y}_o$ ), such that

$$\begin{pmatrix} \mathbf{z}_u \\ \mathbf{r} \\ \mathbf{z}_p \\ \mathbf{y} \end{pmatrix} = \begin{bmatrix} 0 & 0 & 0 & W_u \\ 0 & I & 0 & 0 \\ 0 & W_p & -W_p P_d W_d & -W_p P (I + \Delta W_{in}) \\ W_n & 0 & P_d W_d & P (I + \Delta W_{in}) \end{bmatrix} \begin{pmatrix} \mathbf{n} \\ \mathbf{r} \\ \mathbf{d} \\ \mathbf{u} \end{pmatrix} \quad (15)$$

The weights, which help shape the performance and robustness characteristics of the closed-loop system, include the input weight  $W_{in}(s)$ , the performance weight  $W_p(s)$ , the actuator weight  $W_u(s)$ , the sensor noise weight  $W_n(s)$ , and the disturbance weight  $W_d(s)$ . Now  $W_{in}(s)$  and  $\Delta(s)$ , in Fig. 6, parametrize the uncertainty or errors in the model. The Transfer Function (TF)  $W_{in}(s)$  is assumed known and reflects the amount of uncertainty in the model, whereas the TF  $\Delta(s)$  is assumed complex, full-block, stable, and unknown except for the norm condition  $\|\Delta(s)\|_\infty \leq 1$ . The goal of the controller, synthesized through D-K iteration [89, 90], is to minimize the  $\mathcal{L}_2$ -gain bound  $\gamma$  from the exogenous inputs  $\mathbf{w}$  to the controlled outputs  $\mathbf{z}$ , despite the uncertainty  $\Delta(s)$ .

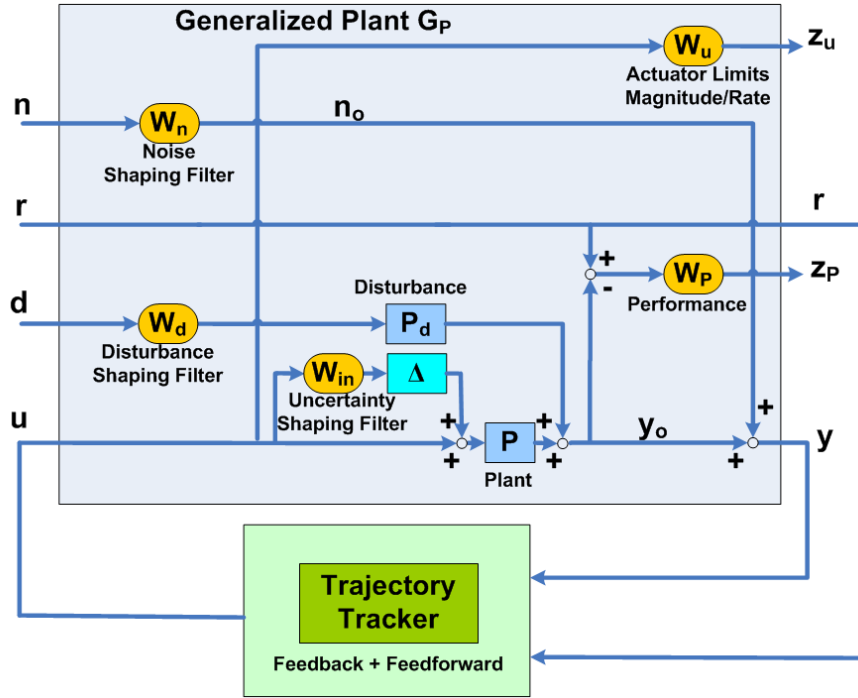


Figure 6: Closed-Loop interconnection structure for robust controller synthesis

The presented TT architecture will be applied twice, once for the inner-loop controller design, and once for the outer-loop controller design.

## 6. Design of the engine OFF inner-loop controller

The inner-loop shall track the following four reference signals: 3D body velocities  $(u \ v \ w)^T$ , and heading angle  $\psi$ . The various signals are further given by: the control inputs  $\mathbf{u} = (\theta_0 \ \theta_{1c} \ \theta_{1s} \ \theta_{TR})^T$ , the reference signals  $\mathbf{r} = (u_{TP} + u_d \ v_{TP} + v_d \ w_{TP} + w_d \ \psi_{TP})^T$ , the system outputs  $\mathbf{y} = (u \ v \ w \ p \ q \ r \ \phi \ \theta \ \psi)^T$ , the wind disturbance signals (given in inertial frame)  $\mathbf{d} = (V_{N_w} \ V_{E_w} \ V_{Z_w})^T$ , and the sensors noise  $\mathbf{n}$  (added to the system outputs), see Fig. 6. To improve the closed-loop performance, the signal  $\mathbf{y}$  contains not only the to-be-tracked signals, but all the available measured output signals, except for the 3D position (since the latter is only of interest for the outer-loop controller).

### 6.1. Choice of nominal plant model for the inner-loop control design

As mentioned in Section 1, this paper does not use any gain-scheduling philosophy, rather a single LTI plant is used for controller design. Now, for an engine ON flight condition, it is relatively easy to find equilibrium points, i.e. steady-state flight conditions, at which the nonlinear helicopter HOM can be linearized. The resulting LTI models can subsequently be used for LTI control design. However, for the engine OFF flight condition, this set of equilibrium points, i.e. steady autorotative flight conditions, is rather small and in certain situations even non-existent. For example, when an engine failure happens at a low altitude, the helicopter does not even reach a steady-state autorotation (corresponding to a constant main rotor RPM), rather the helicopter system is continuously in transition from one non-equilibrium point to the next. To mitigate this problem, the approach used here consists in excluding the main rotor RPM  $\Omega_{MR}$  from the state and measurement vectors, and use this "quasi-steady" modeling approach to find an equilibrium point. Next, the linearization is computed around a zero velocity level flight condition. This condition corresponds to hover, with the engine OFF. Choosing such a flight condition, with an associated velocity of zero, can potentially provide the best description of helicopter behavior during landing (where the helicopter velocity is also very low). A classical numerical perturbation method, resulting in a first-order Taylor series approximation of the nonlinear model (see [56] for further details), is being used. To reduce the controller complexity, a low-order LTI model is being used for the design of the inner-loop trajectory tracker. This LTI model has order nine, containing the following rigid-body states  $\mathbf{x} = (u \ v \ w \ p \ q \ r \ \phi \ \theta \ \psi)^T$ , see Appendix H of Chapter 2 in [56]. By using the eigenvalues of the  $\mathbb{A}$  matrix in the Popov-Belevitch-Hautus (PBH) rank test, it is found that this LTI plant is both controllable and observable.

### 6.2. Selection of weights

The robust control framework makes use of several user-defined weights, see Fig. 6. In this paper, these weights have been chosen as follows. The multiplicative uncertainty weight  $W_{in}(s)$  is of the form  $W_{in}(s) = \text{diag}[w_{in1}(s), w_{in2}(s), w_{in2}(s), w_{in2}(s)]$ , set on the four control input channels  $\mathbf{u} = (\theta_0 \ \theta_{1c} \ \theta_{1s} \ \theta_{TR})^T$ . Further,  $w_{in1}(s)$  and  $w_{in2}(s)$  are filters

whose magnitude represent the relative uncertainty at each frequency (i.e. the level of uncertainty in the behavior of the helicopter is assumed frequency dependent). Based upon engineering judgment<sup>9</sup>, it is chosen here for  $w_{in1}(s)$  to consider 20% uncertainty at low frequency (DC gain), 100% uncertainty at the filter crossover frequency of 10 Hz (with 10 Hz being roughly the anticipated closed-loop bandwidth for the vertical velocity channel), and 200% uncertainty at infinite frequency. Again, based upon engineering judgment, it is chosen for  $w_{in2}(s)$  to consider 40% uncertainty at low frequency (DC gain), 100% uncertainty at the filter crossover frequency of 5 Hz, and 200% uncertainty at infinite frequency, giving

$$\begin{aligned} w_{in1}(s) &= (2s + 22.21)/(s + 111.1) \\ w_{in2}(s) &= (2s + 23.75)/(s + 59.37) \end{aligned} \quad (16)$$

Next, the performance weight filter  $W_p(s)$  is placed on the  $(u, v, w, \psi)$  error signals, to reflect the tracking objective for the three body linear velocities and the heading angle. Here  $W_p(s)$  is a four-by-four, diagonal, frequency-varying weight  $W_p(s) = \text{diag}[w_u(s), w_v(s), w_w(s), w_\psi(s)]$ , with each diagonal term defined as a first-order TF  $\frac{s/M_P + \omega_B}{s + \omega_B A_{ss}}$ . At low frequencies this weighting function should be high in order to keep the error small. Beyond the anticipated bandwidth of the closed-loop system, the tracking error may be released and  $W_p(s)$  rolls off [88]. After several controller design cycles, the weights are defined as

$$\begin{aligned} \text{For } w_u(s) \quad (M_P, \omega_B, A_{ss}) &= (2, 0.5\pi \text{ rad/s}, 0.001) \\ \text{For } w_v(s) \quad (M_P, \omega_B, A_{ss}) &= (2, 0.5\pi \text{ rad/s}, 0.001) \\ \text{For } w_w(s) \quad (M_P, \omega_B, A_{ss}) &= (2, 90\pi \text{ rad/s}, 0.001) \\ \text{For } w_\psi(s) \quad (M_P, \omega_B, A_{ss}) &= (2, 4\pi \text{ rad/s}, 0.001) \end{aligned} \quad (17)$$

This means that a steady-state tracking error of 0.1% with respect to the normalized filter input is allowed. With regard to tracking bandwidth, it is lower on the horizontal channels ( $u$  and  $v$  velocities), since the helicopter nonlinear behavior is

---

<sup>9</sup>Note that the chosen uncertainty may be overly conservative, or may even be unrealistic. Alternative ways to shape the uncertainties exist, see for instance [91]. The goal here is to add some robustness to the closed-loop system.

much more pronounced on the horizontal channels than on the vertical one ( $w$  velocity). Consequently, the helicopter linear behavior on the vertical channel allows to considerably increase the vertical channel bandwidth, as to allow the tracking of a rapidly changing vertical velocity reference. The latter is only feasible if high-bandwidth actuators are mounted on the helicopter (at least for the vertical channel). Now, tracking should not be achieved at the cost of too high control effort. Therefore, both actuator deflection (i.e. amplitude) and rate are penalized through weight  $W_u(s) = \text{diag}[w_{act}(s), w_{act}(s), w_{act}(s), w_{act}(s)]$ , with

$$w_{act}(s) = 10^n \left( \frac{s + \omega_1}{s + \omega_2} \right)^n \quad \text{with} \quad (n, \omega_1, \omega_2) = (3, 40\pi \text{ rad/s}, 400\pi \text{ rad/s}) \quad (18)$$

corresponding to actuators with a bandwidth of approximately 10 Hz. Next, a noise weight  $W_n(s)$  is set to represent the actual noise levels associated with each sensor, and is defined as a nine-by-nine, constant, diagonal scaling matrix described as follows (given here in its unscaled form)

$$W_n(s) = \text{diag}[0.01 \text{ m/s}, 0.01 \text{ m/s}, 0.01 \text{ m/s}, 3\pi/180 \text{ rad/s}, 3\pi/180 \text{ rad/s}, 3\pi/180 \text{ rad/s}, \pi/180 \text{ rad}, \pi/180 \text{ rad}, 3\pi/180 \text{ rad}] \quad (19)$$

Finally, a wind disturbance weight  $W_d(s) = \text{diag}[w_{d_N}(s), w_{d_E}(s), w_{d_D}(s)]$  is added to simulate the frequency content of the NASA Dryden atmospheric wind model<sup>10</sup> [93], resulting in a disturbance bandwidth of 0.06 Hz, 0.12 Hz, and 0.96 Hz along the North, East, and Down (NED) axes respectively. The wind disturbance weights are modeled here, in normalized form, as low-pass filters, as follows

$$\begin{aligned} w_{d_N}(s) &= A_d \frac{s + \omega_1}{s + \omega_2} \quad \text{with} \quad (A_d, \omega_1, \omega_2) = (10^3, 0.22\pi \text{ rad/s}, 2.2\pi \text{ rad/s}) \\ w_{d_E}(s) &= A_d \frac{s + \omega_1}{s + \omega_2} \quad \text{with} \quad (A_d, \omega_1, \omega_2) = (10^3, 0.3\pi \text{ rad/s}, 3\pi \text{ rad/s}) \\ w_{d_D}(s) &= A_d \frac{s + \omega_1}{s + \omega_2} \quad \text{with} \quad (A_d, \omega_1, \omega_2) = (10^3, \pi \text{ rad/s}, 10\pi \text{ rad/s}) \end{aligned} \quad (20)$$

<sup>10</sup>The wind turbulence, or disturbance, frequency content depends upon the mean wind value, and also upon the vehicle height and speed. For the mean wind value, a value of 8 m/s is chosen. This is equivalent to a Beaufort wind force value of 4, corresponding to the yearly average wind force along the coast in The Netherlands [92]. For the vehicle height and speed, it is chosen to have 1 m and 1 m/s respectively, since a low-speed flight condition, close to the ground, results in the highest wind disturbance bandwidth in the NASA Dryden model.



### 6.3. Controller synthesis and analysis

For the D-K iteration [94], one obtains after four iterations a stable controller  $K(s)$  of order 38, using 0<sup>th</sup> order (constant)  $D_s$ -scalings. The controller is further reduced to 30<sup>th</sup> order, after balancing and Hankel-norm model reduction [95], without any significant effect on closed-loop robustness and performance. Fig. 7 visualizes the relevant Transfer Functions (TFs), namely: the output loop TF  $L(s)$ , the input sensitivity  $S_i(s)$ , the output sensitivity  $S_o(s)$ , the input complementary sensitivity  $T_i(s)$ , and the output complementary sensitivity  $T_o(s)$ , with the bandwidths for the three main TFs given in Table 1. In particular, it is seen that the bandwidth of  $|T_i(s)|$  is about equal the bandwidth of the foreseen actuators for our small-scale helicopter, i.e. around 10 Hz. Also the closed-loop disturbance rejection, given in Fig. 8, shows good attenuation of wind disturbances, i.e. approximately -43 dB at a frequency of  $2\pi$  rad/s along the Down axis.

Table 1: Open- and closed-loop bandwidths

Case	Bandwidths (rad/s)		
	$ L(s) $	$ S_i(s) $	$ T_i(s) $
	$w_C$	$w_B$	$w_{BT}$
Engine OFF (Inner-Loop)	35	2.4	65
Engine OFF (Outer-Loop)	3	0.29	6.7

It is observed that  $S_o$  is not well-behaved, since it remains high at both low- and high-frequencies. This can be explained as follows. The output loop  $L(s)$  is a 9x9 matrix, with 4 singular-values having very high values (for low-frequencies). These high singular-values correspond to the 4 controlled channels. Since our helicopter is under-actuated, the remaining 5 singular-values are all very low (for all frequencies). Thus, inverting  $(I + L(s))$  to get  $S_o$  results in maximum singular-values which are most often close to 0 dB. Finally, additional results on Robust Stability (RS) and Robust Performance (RP) can be found in [56].

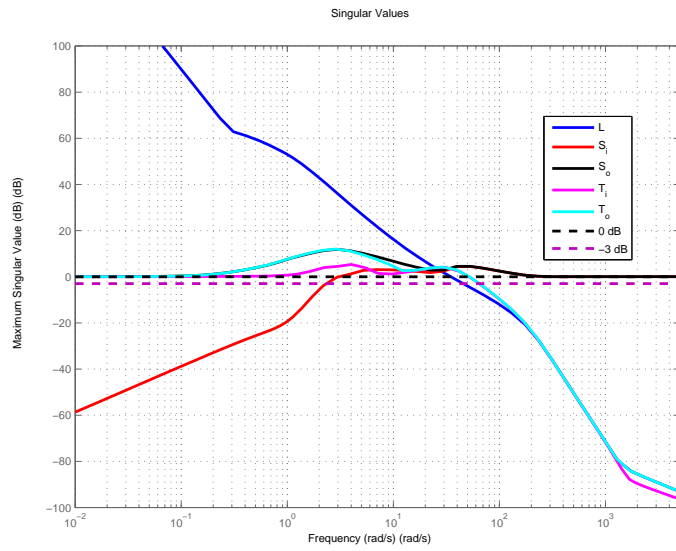


Figure 7: Singular values of  $L(s)$ ,  $S_i(s)$ ,  $S_o(s)$ ,  $T_i(s)$ , and  $T_o(s)$ , of the inner-loop trajectory tracker (Engine OFF case)

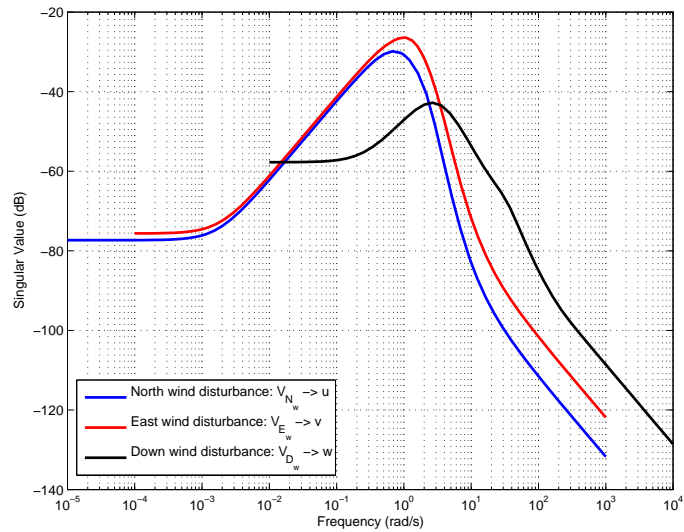


Figure 8: Closed-Loop wind disturbance rejection, for North-East-Down (NED) winds, of the inner-loop trajectory tracker (Engine OFF case)

## 7. Design of the engine OFF outer-loop controller

As mentioned earlier, see Fig. 4, it is chosen to track the following three reference signals: 3D inertial positions  $(x_N \ x_E \ x_Z)^T$ . The various signals are further given as follows: the control inputs  $\mathbf{u} = (V_N \ V_E \ V_Z)_d^T$ , the reference signals  $\mathbf{r} = (x_N \ x_E \ x_Z)_{TP}^T$ , the system outputs  $\mathbf{y} = (x_N \ x_E \ x_Z)^T$ , and the sensors noise  $\mathbf{n}$  (added to the system outputs), see Fig. 6.

### 7.1. Choice of nominal plant model for the outer-loop control design

An LTI dynamical system can be formed by connecting the nominal LTI model, used for the inner-loop TT, with its inner-loop controller, and subsequently adding a set of integrators on the 3D velocities to generate the 3D inertial positions  $(x_N \ x_E \ x_Z)^T$ . This manipulation is readily done in MATLAB, and results in the nominal LTI model needed to design the outer-loop position controller. In our case, a three-by-three input-output system is obtained, with a state-vector of dimension 55. Next a minimum realization is obtained, resulting in a state-vector of dimension 42. Note that here too scalings need to be applied. Further, and except for three poles at the origin (corresponding to the integration of the 3D velocities), all other eigenvalues of the  $\mathbb{A}$  matrix are stable and well damped, implying easier controller design. Again, through the PBH rank test it is found that this LTI system is both controllable and observable.

### 7.2. Selection of weights

The design philosophy for the  $\mu$  outer-loop TT parallels that of the inner-loop. The input multiplicative uncertainty weight  $W_{in}(s)$  is of the form  $W_{in}(s) = \text{diag}[w_{in2}(s), w_{in2}(s), w_{in1}(s)]$ , with  $w_{in1}(s)$ ,  $w_{in2}(s)$  identical to the ones used in the engine OFF inner-loop, in Eq. (16). Here  $w_{in1}(s)$  is set on the vertical velocity channel (recall that  $\mathbf{u} = (V_N \ V_E \ V_Z)_d^T$ ). In the design of the inner-loop TT, in Section 6.2, it is chosen to have an uncertainty weight equal to  $w_{in1}(s)$  on the collective input  $\theta_0$ . Now, since the vertical velocity channel is mostly influenced by the collective input, an uncertainty  $w_{in1}(s)$  to the vertical velocity is also assigned. The same argument holds for uncertainty  $w_{in2}(s)$  on the horizontal velocities. Obviously, this uncertainty choice is somewhat arbitrary.

This said, the purpose here is to add some robustness to the closed-loop system.

The performance weight filter  $W_p(s)$  is placed on the  $(x_N, x_E, x_Z)$  error signals to reflect the tracking objective for the inertial position. Here,  $W_p(s)$  is a three-by-three diagonal, frequency-varying weight. Next,  $W_p(s) = \text{diag}[w_{x_N}(s), w_{x_E}(s), w_{x_Z}(s)]$ , with each diagonal term defined as a first-order transfer function  $\frac{s/M_P + \omega_B}{s + \omega_B A_{ss}}$ . After several controller design cycles, it is settled for

$$\begin{aligned} \text{For } w_{x_N}(s) \quad (M_P, \omega_B, A_{ss}) &= (2, 0.1\pi \text{ rad/s}, 0.001) \\ \text{For } w_{x_E}(s) \quad (M_P, \omega_B, A_{ss}) &= (2, 0.1\pi \text{ rad/s}, 0.001) \\ \text{For } w_{x_Z}(s) \quad (M_P, \omega_B, A_{ss}) &= (2, 4.5\pi \text{ rad/s}, 0.001) \end{aligned} \quad (21)$$

Again, a steady-state tracking error of 0.1% with respect to the normalized input is allowed. The filter bandwidths, on the horizontal channels, are adjusted to be five times smaller than the  $W_p(s)$  filter bandwidths, on the horizontal channels, for the engine OFF inner-loop. For the vertical channel bandwidth, instead of a 1:5 ratio, it is settled for a 1:20 ratio. These values have been obtained after several simulation experiments.

Next, tracking should not be achieved at the cost of too high control effort (i.e. resulting in much too large velocity setpoints  $\mathbf{u} = (V_N \ V_E \ V_Z)_d^T$  for the inner-loop). This means that both inertial velocities and inertial accelerations should be penalized, through weight  $W_u(s) = \text{diag}[w_{act}(s), w_{act}(s), w_{act}(s)]$ , with  $w_{act}(s)$  identical to the one chosen for the inner-loop. Again, this choice may be interpreted as rather arbitrary, since here  $W_u(s)$  is assigned to the inner-loop setpoints  $\mathbf{u} = (V_N \ V_E \ V_Z)_d^T$ , whereas for the design of the inner-loop controller,  $W_u(s)$  was assigned to the actuators. Hence, potentially better choices for  $W_u(s)$  may exist, although the one selected here provided satisfactory results. Finally, a noise weight  $W_n(s)$  is also defined to scale the normalized position measurement noise. The sensor noise model is defined as a three-by-three, constant, diagonal scaling matrix described by (given here in its unscaled form)

$$W_n(s) = \text{diag}[0.1 \ m, 0.1 \ m, 0.1 \ m] \quad (22)$$

### 7.3. Controller synthesis and analysis

For the D-K iteration, after four iterations a stable controller  $K(s)$  of order 57 is obtained, using 0<sup>th</sup> order  $D_s$ -scalings. The controller is further reduced to 30<sup>th</sup> order (using the same technique as for the inner-loop), without any effect on closed-loop robustness/performance. Fig. 9 visualizes the relevant TFs (it is seen that  $S_i(s) = S_o(s)$ , and  $T_i(s) = T_o(s)$ ), with the bandwidths for the three TFs given in Table 1. In particular, it is seen that the bandwidth of  $|T_i(s)|$  is ten times lower its inner-loop counterpart, which is good since one does not want both controllers to start interacting with each other. As for the inner-loop, additional results on Robust Stability (RS) and Robust Performance (RP) can be found in [56].

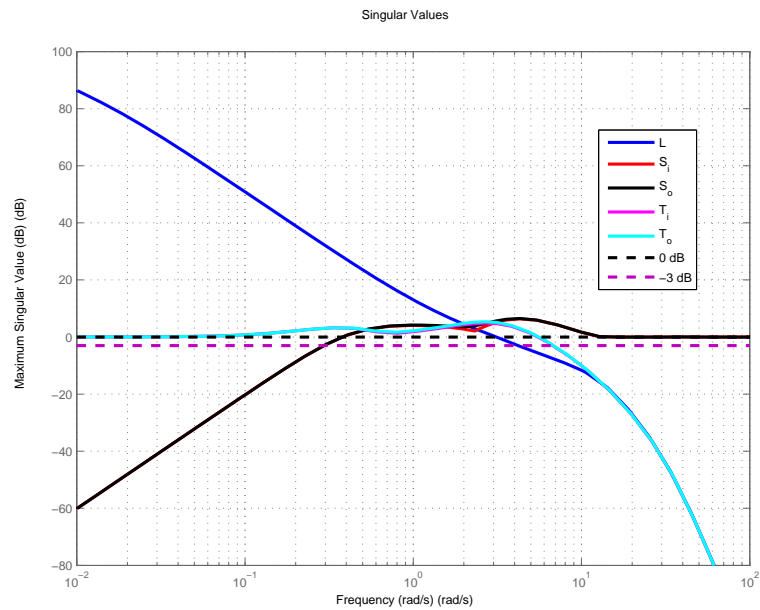


Figure 9: Singular values of  $L(s)$ ,  $S_i(s)$ ,  $S_o(s)$ ,  $T_i(s)$ , and  $T_o(s)$ , of the outer-loop trajectory tracker (Engine OFF case)

### 7.4. Adapting the engine OFF outer-loop controller

When close to the ground, it is crucial to keep the reference velocities as small as possible. To this end, the outer-loop controller is adapted as follows: the position

tracking is switched-off, i.e. the values for  $(u \ v \ w)_d^\top$  are set to zero, once the helicopter height descends below a predefined threshold (keeping only velocity and heading tracking). This helps lowering the final (touch-down) values of the 3D velocities, by giving more time to the velocity deceleration process. The value of this user-defined altitude threshold depends upon the initial conditions (i.e. at the instant of engine shut-down).

## 8. Simulation results

In this section the combined TP and TT functionalities are evaluated. Our nominal LTI inner-loop and outer-loop TT could be applied to other linearized models, as a first step towards controller validation [96, 91]. In this paper, this intermediate step is skipped to go directly to the controller validation on the nonlinear helicopter HOM. Two autorotation (i.e. engine OFF) test cases are presented, starting from different initial conditions. The modeled small-scale UAV is an instrumented Remote-Controlled (RC) Align T-REX helicopter, belonging to the flybarless two-bladed main rotor class. This vehicle has a total mass of 7.75 kg, a main rotor radius of 0.9 m, a main rotor nominal angular velocity of 1350 RPM, a NACA 0015 main rotor airfoil, and an induced velocity in hover given by  $v_{ih} = 3.5$  m/s, see [56] for additional parameters.

The first engine OFF test case is set in an ideal environment, i.e. a noise-free and disturbance-free environment. The purpose of this test case is also to evaluate the FCS performance for an initial flight condition which is not identical to the operating condition at which the LTI model (used for the inner-loop control design) was derived. The second test case is set to illustrate the FCS performance when including sensors measurement noise, together with a wind disturbance.

### 8.1. Setting up the trajectory planning for the engine OFF cases

**Case 1.** This test case involves an autorotation, starting from an engine failure at  $V_N = 8$  m/s, at an altitude of -45 m (the vertical z-axis is oriented positive down), and then landing at 30 m North and 0 m East position, together with a 30° left turn in

heading. Numerically, the initial and final conditions are given by<sup>11</sup>

$$\mathbf{x}_i = \begin{pmatrix} 0 \text{ m} & 0 \text{ m} & -45 \text{ m} & 8 \text{ m/s} & 0 \text{ m/s} & 0 \text{ m/s} & 0 \text{ rad/s} & 0 \text{ rad/s} & 0 \text{ rad/s} & \pi(2.6/180) \text{ rad} & 0 \text{ rad} & -\pi(0.8/180) \text{ rad} \end{pmatrix}^\top$$

$$\mathbf{x}_f = \begin{pmatrix} 30 \text{ m} & 0 \text{ m} & -0.75 \text{ m} & 0 \text{ m/s} & 0 \text{ m/s} & 0.2 \text{ m/s} & 0 \text{ rad/s} & 0 \text{ rad/s} & 0 \text{ rad/s} & 0 \text{ rad} & 0 \text{ rad} & -\pi(30/180) \text{ rad} \end{pmatrix}^\top$$

Here, the following comments are made

- A final value to the North and East horizontal positions is given. This represents additional constraints on the TP. This is done with an eye on future experimental flight tests where, for safety reasons, one wants to know beforehand where the helicopter will be landing.
- The final altitude  $x_Z$  (see the third component of  $\mathbf{x}_f$ ) is set to -0.75 m. This allows to add a safety margin into the planned trajectory.
- The final vertical velocity  $w$  (see the sixth component of  $\mathbf{x}_f$ ) is set to 0.2 m/s. When close to the ground, the goal is to move at a constant and slow rate of descent (until the skids hit the ground).

Next, the flight envelope (i.e. state constraints in the form of minimum and maximum limits, partially based upon engineering judgment) is defined as follows

$$\mathbf{x}_{min} = - \begin{pmatrix} 50 \text{ m} & 50 \text{ m} & 50 \text{ m} & 5 \text{ m/s} & 1 \text{ m/s} & 3 \text{ m/s} & \pi(100/180) \text{ rad/s} & \pi(100/180) \text{ rad/s} & \pi(100/180) \text{ rad/s} & \pi(15/180) \text{ rad} & \pi(15/180) \text{ rad} & 2\pi \text{ rad} \end{pmatrix}^\top$$

$$\mathbf{x}_{max} = \begin{pmatrix} 50 \text{ m} & 50 \text{ m} & -0.25 \text{ m} & 15 \text{ m/s} & 1 \text{ m/s} & 15 \text{ m/s} & \pi(100/180) \text{ rad/s} & \pi(100/180) \text{ rad/s} & \pi(100/180) \text{ rad/s} & \pi(15/180) \text{ rad} & \pi(15/180) \text{ rad} & 2\pi \text{ rad} \end{pmatrix}^\top$$

Here, the following comments are made

<sup>11</sup>Recall also that the rigid-body dynamics, used in the flatness TP, is characterized by a state-vector of dimension twelve  $\mathbf{x} = (x_N \ x_E \ x_Z \ u \ v \ w \ p \ q \ r \ \phi \ \theta \ \psi)^\top$ , with total forces and total moments as inputs, each of dimension three, given by  $\mathbf{F}_{CG}^b = (F_{CG_X}^b \ F_{CG_Y}^b \ F_{CG_Z}^b)^\top$ , and  $\mathbf{M}_{CG}^b = (M_{CG_X}^b \ M_{CG_Y}^b \ M_{CG_Z}^b)^\top$ .

- When the helicopter is on the ground, the CG height is equal to -0.25 m (see the third component of  $\mathbf{x}_{max}$ ).
- Vehicle operation beyond 15 m/s is not foreseen (fourth component of  $\mathbf{x}_{max}$ ).
- The body lateral velocity  $v$  is constrained to  $\pm 1$  m/s, as to limit vehicle sideslip.
- The roll  $\phi$  and pitch  $\theta$  angles are limited to  $\pm 15^\circ$ , in order to: 1) keep the load factor  $n$  within acceptable values, i.e. preferably below one; and 2) minimize the system's nonlinear behavior, facilitating thus the trajectory tracking.

Next, the input constraints, i.e. on the total forces and total moments, are based upon simulation experiments with the nonlinear helicopter HOM, and have been chosen as

$$\mathbf{F}_{CG_{min}}^b = - \begin{pmatrix} 20 \text{ N} & 15 \text{ N} & 120 \text{ N} \end{pmatrix}^\top \quad \mathbf{M}_{CG_{min}}^b = - \begin{pmatrix} 5 \text{ Nm} & 5 \text{ Nm} & 5 \text{ Nm} \end{pmatrix}^\top$$

$$\mathbf{F}_{CG_{max}}^b = \begin{pmatrix} 20 \text{ N} & 15 \text{ N} & -30 \text{ N} \end{pmatrix}^\top \quad \mathbf{M}_{CG_{max}}^b = \begin{pmatrix} 5 \text{ Nm} & 5 \text{ Nm} & 5 \text{ Nm} \end{pmatrix}^\top$$

Besides, in the cost functional of Section 4.3.1, the following weights  $W_u = W_v = W_w = W_\psi = 1$  have been used. Additional constraints have also been included, namely a tail rotor blade tip clearance to avoid ground strike by the tail rotor during flare (see [86] for more details). Also, the final time  $T_f$  is bounded such that  $T_f \leq T_{OFF}$ , with  $7.3 \text{ s} \leq T_{OFF} \leq 8.5 \text{ s}$ . Here a value of  $T_{OFF} = 7.3 \text{ s}$  is chosen.

For high initial velocity conditions, the following 'adaptation' for the outer-loop controller has been used. When  $|x_Z| \leq 5 \text{ m}$  is true, the horizontal position tracking ( $x_N, x_E$ ) is stopped. This helps to lower the final values of the 2D horizontal velocities. Further, when  $|x_Z| \leq 1 \text{ m}$  is true, the vertical position tracking ( $x_Z$ ) is stopped as well.

**Case 2.** This test case involves an autorotation, starting from an engine failure in hover, at an altitude of -30 m, and then landing at 0 m North and 0 m East position (i.e. the horizontal position of the landing spot is identical to the horizontal position of the initial state), without any heading turn. Gaussian white noise is added on the 12



measured states  $\mathbf{y} = (x_N \ x_E \ x_Z \ u \ v \ w \ p \ q \ r \ \phi \ \theta \ \psi)^\top$ , with the following 1- $\sigma$  values

$$\begin{pmatrix} 0.1 \text{ m} & 0.1 \text{ m} & 0.1 \text{ m} & 0.05 \text{ m/s} & 0.05 \text{ m/s} & 0.05 \text{ m/s} \\ \pi(3/180) \text{ rad} & \pi(3/180) \text{ rad} & \pi(3/180) \text{ rad} \\ \pi(1/180) \text{ rad} & \pi(1/180) \text{ rad} & \pi(3/180) \text{ rad} \end{pmatrix}^\top$$

These 1- $\sigma$  values correspond to the noise weight values used during controller design, except for the noise on the three body velocities (the three most critical signals) where a noise value which is five times higher than the value used during controller design has been used, in order to better visualize the response characteristics of the FCS. A headwind of 8 m/s is also included, which is equivalent to a Beaufort wind force value of 4, corresponding to the yearly average wind force along the coast in The Netherlands [92]. Note that this is a rather heavy wind condition for such a small-scale helicopter. Now, numerically, the initial and final conditions for this maneuver are given by

$$\begin{aligned} \mathbf{x}_i &= \begin{pmatrix} 0 \text{ m} & 0 \text{ m} & -30 \text{ m} & 0 \text{ m/s} & 0 \text{ m/s} & 0 \text{ m/s} \\ 0 \text{ rad/s} & 0 \text{ rad/s} & 0 \text{ rad/s} & \pi(3.4/180) \text{ rad} & 0 \text{ rad} & 0 \text{ rad} \end{pmatrix}^\top \\ \mathbf{x}_f &= \begin{pmatrix} 0 \text{ m} & 0 \text{ m} & -0.75 \text{ m} & 0 \text{ m/s} & 0 \text{ m/s} & 0.2 \text{ m/s} \\ 0 \text{ rad/s} & 0 \text{ rad/s} & 0 \text{ rad/s} & 0 \text{ rad} & 0 \text{ rad} & 0 \text{ rad} \end{pmatrix}^\top \end{aligned}$$

The final time  $T_f$  is bounded such that  $T_f \leq T_{OFF}$ , with  $4.9\text{s} \leq T_{OFF} \leq 5.7\text{s}$ . Here a value  $T_{OFF} = 5 \text{ s}$  is chosen. Regarding the state and input constraints, and cost functional weights, together with the 'adaptation' functionality of the outer-loop controller, these are identical to the engine OFF case 1.

**Remark 5.** *A direct feedthrough from the planning module to the tracking controller does exist, but this is of no concern since the model-based TP designs position and velocity references that are in accordance with the time-scale separation. A further check shows that the frequency content of the various inner- and outer-loop reference signals (generated by the TP for both test cases) are indeed lower than the corresponding bandwidth of the complementary sensitivity function  $T_i(s)$ , as reported in Table 1. Hence the TT ought to be able to track these reference signals.*

## 8.2. Discussion of closed-loop simulation results

Fig. 10 and Fig. 11 visualize the evolution of the 3D inertial velocities ( $V_N, V_E, V_Z$ ) and positions ( $x_N, x_E, x_Z$ ). Although the vertical z-axis is oriented positive down, in these figures  $V_Z$  and  $x_Z$  are shown positive up for better readability.

Further, Fig. 12 and Fig. 13 visualize the time-histories for the body states, namely attitude angles ( $\phi, \theta, \psi$ ), linear velocities ( $u, v, w$ ), and rotational velocities ( $p, q, r$ ). Here, the black lines represent the outputs from the flatness TP, these include the planned 3D inertial positions  $(x_N \ x_E \ x_Z)_{TP}^T$ , defined in Fig. 4, the planned 3D body velocities  $(u \ v \ w)_{TP}^T$ , defined in Fig. 5, and the planned heading  $\psi_{TP}$ , also defined in Fig. 5. The flatness-based TP, in Section 4, computes also a planned trajectory for the remaining states, e.g. roll angle  $\phi$ , pitch angle  $\theta$ , roll rate  $p$ , etc. However, and for the sake of clarity, in Fig. 10, Fig. 11, Fig. 12, and Fig. 13, only the TP outputs that will eventually be tracked have been visualized.

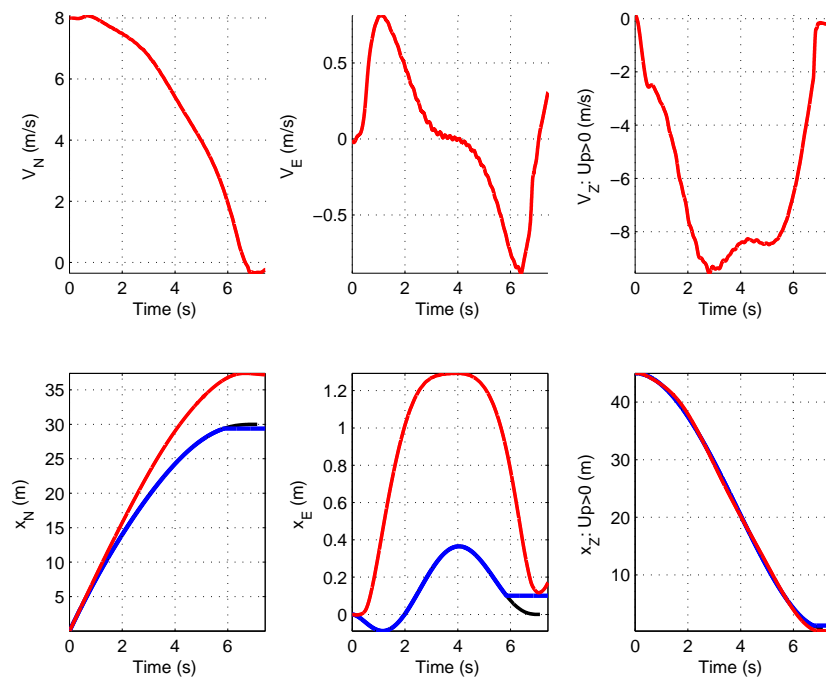


Figure 10: Inertial velocities and positions, for the Engine OFF case 1. Black line: flatness planning. Blue line: references for outer-loop. Red line: controlled nonlinear model

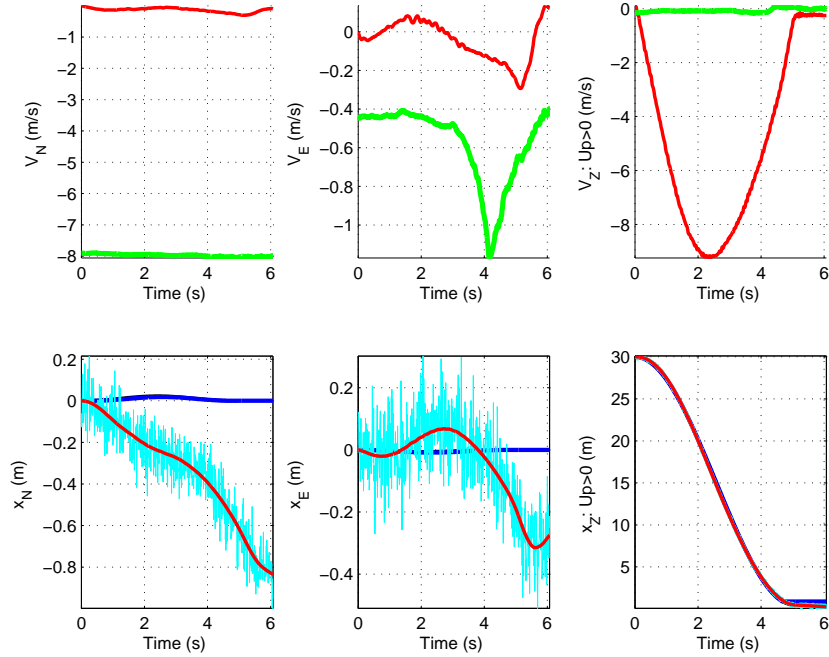


Figure 11: Inertial velocities and positions, for the Engine OFF case 2. Black line: flatness planning. Blue line: references for outer-loop. Red line: controlled nonlinear model. Cyan line: noisy measurements. Green line: wind disturbance.

In Fig. 10 and Fig. 11, the blue lines, named *reference for outer-loop*, represent the signals that need to be tracked by the outer-loop controller. Here, these signals are simply the planned 3D inertial positions  $(x_N \ x_E \ x_Z)_{TP}^T$ , i.e. black and blue lines are identical (except at the end of the flight, where position control is stopped, see Section 7.4). In Fig. 12 and Fig. 13, the blue lines, named *reference for inner-loop*, represent the signals that need to be tracked by the inner-loop controller. Here, these signals include the planned heading  $\psi_{TP}$ , where again black and blue lines are identical. However, the velocities that need to be tracked by the inner-loop are given by  $(u \ v \ w)_{TP}^T + (u \ v \ w)_d^T$ , and hence black and blue lines are not identical. Further, the red lines represent the outputs from the nonlinear helicopter HOM. In Fig. 11 and Fig. 13 the corresponding noisy measurement signals, sent to the inner- and outer-loop controllers, are visualized in cyan. In Fig. 11 the wind disturbance is visualized in green. This wind disturbance includes a constant (deterministic) headwind of 8 m/s, together with a small gust (Dry-

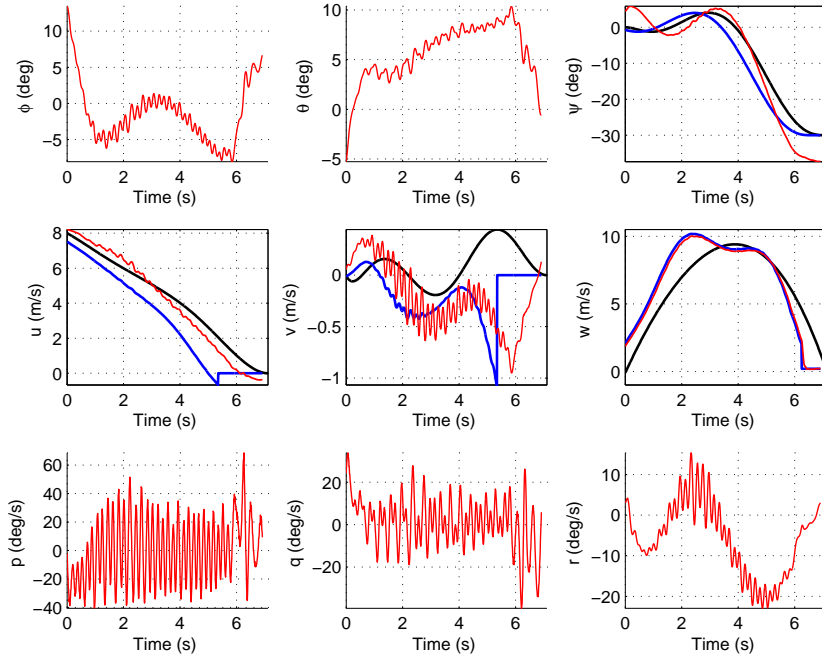


Figure 12: Euler angles, body linear velocities, and body rotational velocities, for the Engine OFF case 1. Black line: flatness planning. Blue line: references for inner-loop. Red line: controlled nonlinear model

den stochastic variation) on the three linear axes. Finally, Fig. 14 and Fig. 15 visualize the required control inputs for the engine OFF test cases 1 and 2 respectively, whereas Fig. 16 and Fig. 17 visualize the time-histories for the main rotor RPM  $\Omega_{MR}$ . From all these figures, it is observed that:

- The combined trajectory planning and tracking system is capable of safely guiding and controlling the helicopter in autorotation.
- The specifications for a successful automatic landing, see Definition 2 in Section 4.3.2, have been defined as  $|u| \leq 0.5$  m/s,  $|v| \leq 0.5$  m/s,  $|w| \leq 0.25$  m/s,  $|\phi| \leq 10^\circ$ , and  $|\theta| \leq 10^\circ$ . For case 1, at the instant of ground impact, the following values are observed: the body horizontal velocities  $u = -0.37$  m/s,  $v = 0.13$  m/s, the body vertical velocity  $w = 0.21$  m/s, and the roll and pitch angles  $\phi = 6.67^\circ$ , and  $\theta = -0.54^\circ$ . For case 2, the following values are found: for the body horizontal velocities  $u = -0.09$  m/s,  $v = 0.12$  m/s, the body vertical

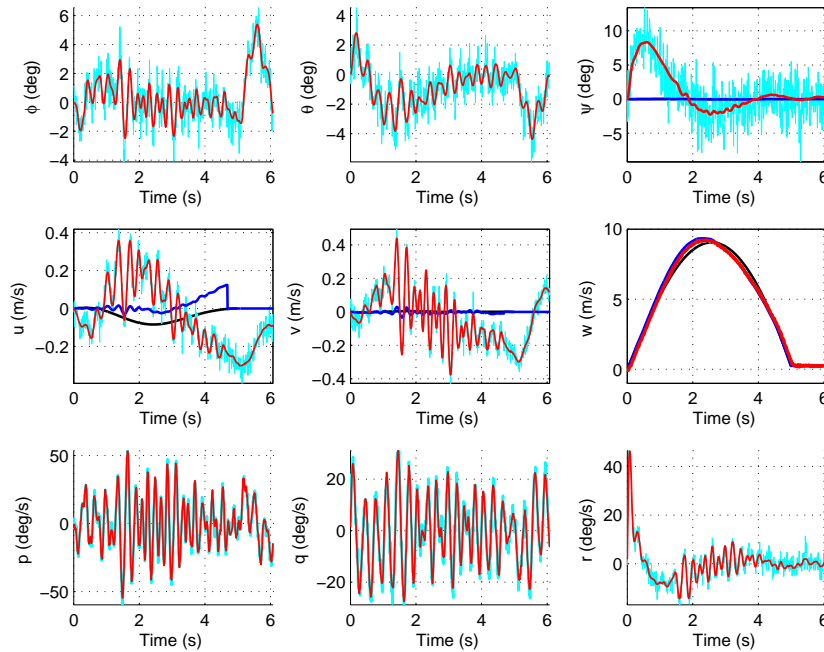


Figure 13: Euler angles, body linear velocities, and body rotational velocities, for the Engine OFF case 2. Black line: flatness planning. Blue line: references for inner-loop. Red line: controlled nonlinear model. Cyan line: noisy measurements.

velocity  $w = 0.24$  m/s, and the roll and pitch angles  $\phi = -0.75^\circ$ , and  $\theta = -0.15^\circ$ . Hence all specifications for a successful automatic landing are met.

- A single LTI controller is capable of controlling and landing the helicopter system, in autorotation, for a relatively large variation in forward and vertical vehicle velocity (at least up to approximately 8 to 10 m/s), and for relatively large variations in main rotor RPM (approximately in the range 70% to 110% of the nominal engine ON value), see Fig. 12, Fig. 13, Fig. 16, and Fig. 17.
- Tracking performance is better for the vertical motion  $w$  and  $x_Z$ , than the tracking of horizontal motion  $(u, v)$  and  $(x_N, x_E)$ .
- Some steady-state errors can be seen on the horizontal channel (see Fig. 10 and Fig. 11) and heading (see Fig. 12 and Fig. 13), whereas this is not the case for the vertical channel (refer to these same figures). This is also partially due to the

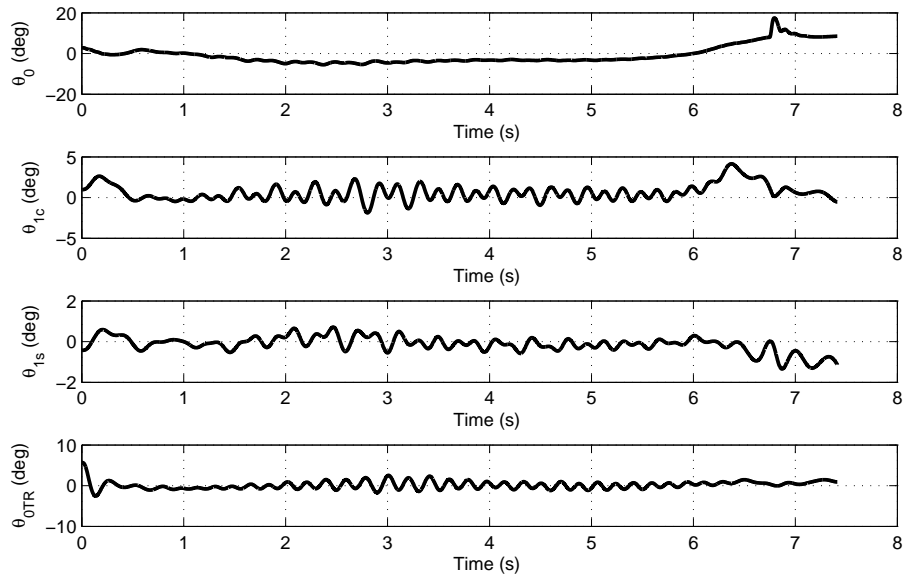


Figure 14: Helicopter control inputs, for the Engine OFF case 1

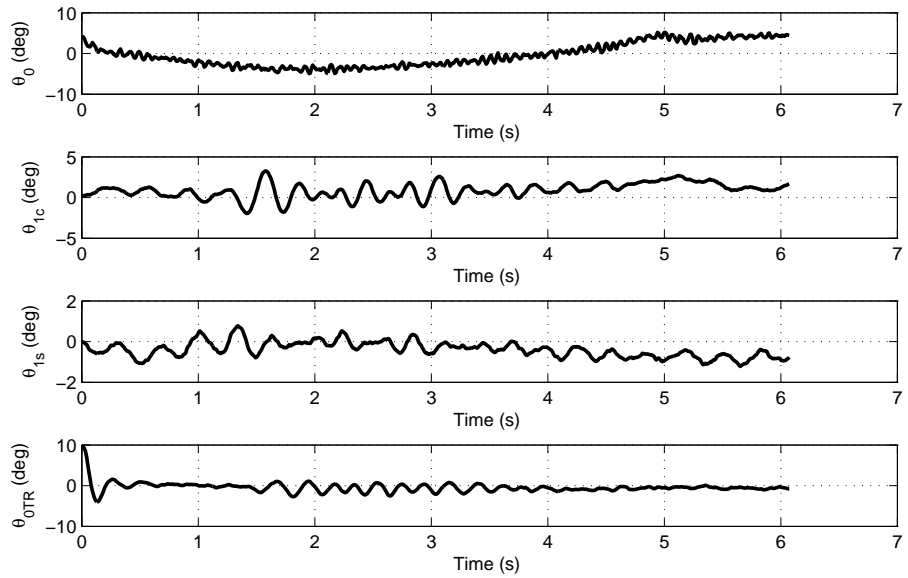


Figure 15: Helicopter control inputs, for the Engine OFF case 2

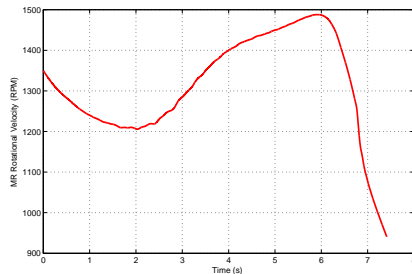


Figure 16: Main rotor RPM  $\Omega_{MR}$ , for the Engine OFF case 1

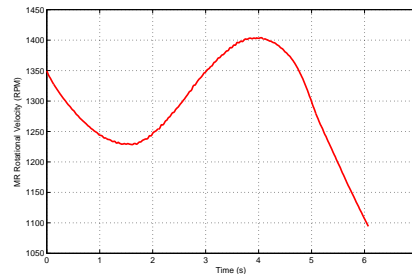


Figure 17: Main rotor RPM  $\Omega_{MR}$ , for the Engine OFF case 2

fact that position control is stopped some time before the helicopter touches the ground (see our discussion in Section 7.4).

- Although the nominal model, used for control design, was linearized at a condition outside the ground effect, no performance deterioration of the closed-loop system was noticed when the helicopter was in ground effect.
- The FCS has shown good performance with respect to sensors noise and wind disturbance (albeit only one example is shown here), see Fig. 11 and Fig. 13.

## 9. Conclusion

This paper demonstrates a, model-based, automatic safety recovery system that could safely fly and land a small-scale helicopter UAV in un-powered flight (i.e. autorotation). The presented flight control solution incorporates a classic guidance and control logic, in which the guidance module is decoupled from the control module. The goal of the guidance module, or Trajectory Planning (TP), is to generate open-loop, feasible and optimal autorotative trajectories, for the helicopter, whereas the aim of the control module, or Trajectory Tracking (TT), consists in enabling the helicopter to fly along these optimal trajectories. The work presented in this paper resulted in the first demonstration of a, real-time feasible, model-based TP and model-based TT, for the case of a small-scale helicopter UAV, in autorotation. The validation was performed using a high-fidelity helicopter simulation, based upon a nonlinear, High-Order Model

(HOM). Our results showed that the crucial control of vertical position and velocity exhibited outstanding behavior in terms of tracking performance, and did not require any additional increase in control bandwidth. However, the tracking of horizontal positions and horizontal velocities was clearly lacking some bandwidth. Unfortunately, a further increase of the horizontal closed-loop bandwidths resulted in closed-loop instabilities, when evaluated on the nonlinear helicopter HOM. Hence, the horizontal channel tracking performance could potentially be improved by considering one of the following options for the TT: 1) remaining in the framework of Linear Time-Invariant (LTI) control, however with the use of a higher-order LTI plant for control design (containing the main rotor dynamics), instead of the low-order plant used in this paper; or 2) using a more sophisticated control method, which better exploits the system's nonlinear structure, such as nonlinear, adaptive, or Linear Parameter-Varying (LPV) methods.



## Appendix A: nomenclature

Vectors are printed in boldface  $\mathbf{X}$ . A vector is qualified by its subscript, whereas its superscript denotes the projection frame: e.g.  $\mathbf{V}_a^I$  represents the aerodynamic velocity projected on frame  $F_I$ . Matrices are written in outline type  $\mathbb{M}$ , and transformation matrices are denoted as  $\mathbb{T}_{ij}$ , with the two suffices signifying from frame  $F_j$  to frame  $F_i$ . All units are in the S.I. system.

Frame names (these are the standard aircraft navigation frames [97])

$F_I$	Geocentric inertial frame
$F_o$	Vehicle carried normal earth frame
$F_b$	Body (vehicle) frame
$F_k$	Kinematic (flight path) frame

Positions and Angles

$x_N, x_E, x_Z$	Coordinates of vehicle CG
$\phi$	Vehicle bank angle (roll angle)
$\theta$	Vehicle inclination angle (pitch angle, or elevation)
$\psi$	Vehicle azimuth angle (yaw angle, heading)
$\psi_f$	Wind heading angle

Linear velocities  $\mathbf{V}$  and their components  $u, v, w$

$\mathbf{V}_{k,G}$	Kinematic velocity of vehicle CG
$\mathbf{V}_{a,G}$	Aerodynamic velocity of vehicle CG
$u_k^o = V_N$	$x$ component of $\mathbf{V}_{k,G}$ on $F_o$ , North velocity
$v_k^o = V_E$	$y$ component of $\mathbf{V}_{k,G}$ on $F_o$ , East velocity
$w_k^o = V_Z$	$z$ component of $\mathbf{V}_{k,G}$ on $F_o$ , Vertical velocity
$u_k^b = u$	$x$ component of $\mathbf{V}_{k,G}$ on $F_b$
$v_k^b = v$	$y$ component of $\mathbf{V}_{k,G}$ on $F_b$
$w_k^b = w$	$z$ component of $\mathbf{V}_{k,G}$ on $F_b$
$u_w$	Wind $x$ -velocity in $F_E$
$v_w$	Wind $y$ -velocity in $F_E$
$w_w$	Wind $z$ -velocity in $F_E$

Angular velocities  $\Omega$  and their components  $p, q, r$

$\Omega_k = \Omega_{bE}$  Kinematic angular velocity of vehicle CG relative to the earth

$p_k^b = p$  Roll velocity (roll rate) of vehicle CG wrt to the earth

$q_k^b = q$  Pitch velocity (pitch rate) of vehicle CG wrt to the earth

$r_k^b = r$  Yaw velocity (yaw rate) of vehicle CG wrt to the earth

Main Rotor (MR) properties

$\beta_{bl}$  Blade flap angle

$\beta_{1s}$  Lateral rotor TPP tilt

$\Gamma$  MR rotation,  $CCW : \Gamma = 1$ .  $CW : \Gamma = -1$

$I_b$  Blade 2nd mass moment (inertia about rotor shaft)

$M_{bl}$  Blade mass from flap hinge

$N_b$  Number of blades

$\Omega_{MR}$  Instantaneous angular velocity

$\Omega_{MR100\%}$  Nominal (100%) angular velocity

$R_{rot}$  Rotor radius measured from hub center

Control Inputs

$\theta_0$  MR blade root collective pitch

$\theta_{1c}$  MR lateral cyclic pitch

$\theta_{1s}$  MR longitudinal cyclic pitch

$\theta_{TR}$  TR blade collective pitch angle

Miscellaneous

$g$  Acceleration due to gravity

$m_V$  Vehicle mass

$\mathbb{I}_V = \begin{bmatrix} A & -F & -E \\ -F & B & -D \\ -E & -D & C \end{bmatrix}$  Vehicle inertia matrix

## References

- [1] S. Taamallah, A qualitative introduction to the vortex-ring-state, autorotation, and optimal autorotation, in: Europ. Rotorcraft Forum, 2010.
- [2] D. Santamara, A. Viguria, M. Bejar, K. Kondak, A. Ollero, Towards autonomous autorotation landing for small size unmanned helicopters, *J. Intell. Robot Syst.* 69 (1-4) (2013) 171–180.
- [3] S. Taamallah, A flight dynamics model for a small-scale flybarless helicopter, *ASME J. of Dynamic Systems Measurement and Control* 138 (2016) 1–20.
- [4] P. Abbeel, A. Coates, T. Hunter, A. Y. Ng, Autonomous autorotation of an rc helicopter, in: 11th Int. Symposium on Experimental Robotics (ISER), 2008.
- [5] J. Holsten, S. Loechelt, W. Alles, Autonomous autorotation flights of helicopter uavs to known landing sites, in: Am. Helicopter Soc., 2010.
- [6] T. Yomchinda, J. F. Horn, J. W. Langelaan, Autonomous control and path planning for autorotation of unmanned helicopters, in: Am. Helicopter Soc., 2012.
- [7] Z. Sunberg, J. Rogers, A fuzzy logic-based controller for helicopter autorotation, in: AIAA Aerospace Sciences Meeting and Exhibit, 2013.
- [8] W. Johnson, Helicopter optimal descent and landing after power loss, Tech. Rep. TM 73-244, NASA Ames Research Center (1977).
- [9] A. Lee, Engineering notes - optimal autorotational descent of a helicopter with control and state inequality constraints, *AIAA J. of Guidance, Control, and Dynamics* 13 (5) (1990) 922–924.
- [10] Y. Okuno, K. Kawachi, Optimal control of helicopters following power failure, *AIAA J. of Guidance, Control, and Dynamics* 17 (1) (1994) 181–186.
- [11] B. L. Aponso, E. N. Bachelder, D. Lee, Automated autorotation for unmanned rotorcraft recovery, in: AHS Int. Specialists' Meeting On Unmanned Rotorcraft, 2005.

- [12] C. L. Bottasso, A. Croce, D. Leonello, L. Riviello, Optimization of critical trajectories for rotorcraft vehicles, *J. of the Am. Helicopter Soc.* (2005) 165–177.
- [13] M. W. Floros, Application of sequential quadratic programming to rotorcraft survivability with power loss, in: *Am. Helicopter Soc.*, 2011.
- [14] P. Bibik, J. Narkiewicz, Helicopter optimal control after power failure using comprehensive dynamic model, *AIAA J. of Guidance, Control, and Dynamics* 35 (4) (2012) 1354–1362.
- [15] M. Fliess, Generalized controller canonical forms for linear and nonlinear dynamics, *IEEE Trans. Autom. Control* 35 (1990) 994–1001.
- [16] D. H. Shim, H. J. Kim, S. Sastry, Hierarchical control system synthesis for rotorcraft-based unmanned aerial vehicles, in: *AIAA Guidance, Navigation and Control Conf.*, 2000.
- [17] M. Takahashi, G. Schulein, M. Whalley, Flight control law design and development for an autonomous rotorcraft, in: *Am. Helicopter Soc.*, 2008.
- [18] M. Bergerman, O. Amidi, J. Miller, N. Vallidis, T. Dudek, Cascaded position and heading control of a robotic helicopter, in: *Int. Conf. on Intelligent Robots and Systems*, 2007.
- [19] K. Nonami, F. Kendoul, S. Suzuki, W. Wang, D. Nakazawa, *Autonomous Flying Robots - Unmanned Aerial Vehicles and Micro Aerial Vehicles*, Springer, New York, 2010.
- [20] J. Shin, K. Nonami, D. Fujiwara, K. Hazawa, Model-based optimal attitude and positioning control of small-scale unmanned helicopter, *Robotica* 23 (2005) 51–63.
- [21] G. M. Voorluis, Parameter-dependent robust control for a rotorcraft uav, in: *AIAA Guidance, Navigation and Control Conf.*, 2005.
- [22] M. F. Weilenmann, U. Christen, H. P. Geering, Robust helicopter position control at hover, in: *Am. Control Conf.*, 1994.

- [23] M. L. Civita, Integrated modeling and robust control for full-envelope flight of robotic helicopters, Ph.D. thesis, Carnegie Mellon University (2002).
- [24] J. Gadewadikar, F. L. Lewis, K. Subbarao, B. M. Chen, Structured  $h_\infty$  command and control-loop design for unmanned helicopters, *AIAA J. of Guidance, Control, and Dynamics* 31 (4) (2008) 1093–1102.
- [25] Y. Q. He, J. D. Han, Acceleration-feedback-enhanced robust control of an unmanned helicopter, *AIAA J. of Guidance, Control, and Dynamics* 33 (4) (2010) 1236–1250.
- [26] D. H. Shim, T. J. Koo, F. Hoffmann, S. Sastry, A comprehensive study on control design of autonomous helicopter, in: *IEEE Conf. on Decision and Control*, 1998.
- [27] H. J. Kim, D. H. Shim, A flight control system for aerial robots: Algorithms and experiments, *Control Engineering Practice* 11 (12) (2003) 1389–1400.
- [28] D. H. Shim, S. Sastry, A situation-aware flight control system design using real-time model predictive control for unmanned autonomous helicopters, in: *AIAA Guidance, Navigation, and Control Conf.*, 2006.
- [29] A. Isidori, L. Marconi, A. Serrani, Robust nonlinear motion control of a helicopter, *IEEE Trans. Autom. Control* 40 (3) (2003) 413–426.
- [30] K. Peng, G. Cai, B. M. Chen, M. Dong, K. Y. Luma, T. H. Lee, Design and implementation of an autonomous flight control law for a uav helicopter, *Automatica* 45 (2009) 2333–2338.
- [31] P. Simplicio, M. D. Pave, E. vanKampen, Q. P. Chu, An acceleration measurements-based approach for helicopter nonlinear flight control using incremental nonlinear dynamic inversion, *Control Engineering Practice* 21 (2013) 1065–1077.
- [32] E. N. Johnson, S. K. Kannan, Adaptive trajectory control for autonomous helicopters, *AIAA J. of Guidance, Control, and Dynamics* 28 (3).

- [33] I. Yavrucuk, J. V. R. Prasad, S. Unnikrishnan, Envelope protection for autonomous unmanned aerial vehicles, *AIAA J. of Guidance, Control, and Dynamics* 32 (1) (2009) 248–261.
- [34] B. J. Guerreiro, C. Silvestre, R. Cunha, C. Cao, N. Hovakimyan, L1 adaptive control for autonomous rotorcraft, in: *Am. Helicopter Soc.*, 2009.
- [35] M. Bisgaard, A. Cour-Harbo, J. D. Bendtsen, Adaptive control system for autonomous helicopters slung load operations, *Control Engineering Practice* 18 (2010) 800–811.
- [36] V. Gavrilets, E. Frazzoli, B. Mettler, E. Feron, Aggressive maneuvering of small autonomous helicopters: A human-centered approach, *Int. J. of Robotics Research* 20.
- [37] A. Y. Ng, A. Coates, M. Diel, V. Ganapathi, J. Schulte, B. Tse, E. Berger, E. Liang, Autonomous inverted helicopter flight via reinforcement learning, in: *Int. Symposium on Experimental Robotics*, 2004.
- [38] P. Abbeel, A. Coates, M. Quigley, A. Y. Ng, An application of reinforcement learning to aerobatic helicopter flight, in: *NIPS 19*, 2007.
- [39] G. Zames, On the input-output stability of time-varying nonlinear feedback systems-part i: Conditions derived using concepts of loop gain, conicity, and positivity, *IEEE Trans. Autom. Control* AC-11 (1966) 228–238.
- [40] C. A. Desoer, M. Vidyasagar, *Feedback Systems: Input-Output Properties*, Academic Press, New York, 1975.
- [41] E. Seckel, H. C. Curtiss, Aerodynamic characteristics of helicopter rotors, *Tech. Rep. No. 659*, Department of Aerospace and Mechanical Engineering, Princeton University (1962).
- [42] R. T. N. Chen, A simplified rotor system mathematical model for piloted flight dynamics simulation, *Tech. Rep. NTM 78575*, NASA Ames Research Center (1979).

- [43] R. T. N. Chen, Effects of primary rotor parameters on flapping dynamics, Tech. Rep. NTP 1431, NASA Ames Research Center (1980).
- [44] G. D. Padfield, Helicopter Flight Dynamics, Blackwell Science Ltd, Oxford, UK, 1996.
- [45] A. Gessow, G. C. Myers, Aerodynamics of the Helicopter, College Park Pr, 1999.
- [46] D. M. Pitt, D. A. Peters, Theoretical prediction of dynamic-inflow derivatives, in: Europ. Rotorcraft Forum, 1980.
- [47] D. A. Peters, N. HaQuang, Technical notes - dynamic inflow for practical applications, J. of the Am. Helicopter Soc. (1988) 64–68.
- [48] D. A. Peters, C. He, Technical note: Modification of mass-flow parameter to allow smooth transition between helicopter and windmill states, J. of the Am. Helicopter Soc. (2006) 275–278.
- [49] R. S. Shevell, Fundamentals of Flight, Prentice Hall, Upper Saddle River NJ, 1989.
- [50] J. D. Anderson, Fundamentals of Aerodynamics. Third Ed., McGraw-Hill Higher Education, NY, 2001.
- [51] R. W. Prouty, Helicopter Performance, Stability, and Control, Krieger Publishing Company, Malabar, Florida USA, 1995.
- [52] D. A. Peters, C. J. He, Finite state induced flow models part ii: Three-dimensional rotor disk, AIAA J. of Aircraft 32 (2) (1995) 323–333.
- [53] R. T. N. Chen, Flap-lag equations of motion of rigid, articulated rotor blades with three hinge sequences, Tech. Rep. NTM 100023, NASA Ames Research Center (1987).
- [54] F. J. Bailey, A simplified theoretical method of determining the characteristics of a lifting rotor in forward flight, Tech. Rep. RNo. 716, NACA (1941).
- [55] ART, <http://www.flightlab.com/>, Mountain View CA., U.S.A.

- [56] S. Taamallah, Small-scale helicopter automatic autorotation: Modeling, guidance, and control, Ph.D. thesis, Delft University of Technology (2015).
- [57] M. Fliess, J. Levine, P. Martin, P. Rouchon, Flatness and defect of nonlinear systems: Introductory theory and examples, *Int. J. of Control* 61 (6) (1995) 1327–1361.
- [58] H. Sira-Ramirez, S. K. Agrawal, *Differentially Flat Systems*, Marcel Dekker Inc., 2004.
- [59] J. Levine, *Analysis and Control of Nonlinear Systems: A Flatness-Based Approach*, Springer, 2009.
- [60] I. M. Ross, F. Fahroo, A unified computational framework for real-time optimal control, in: *IEEE Conf. on Decision and Control*, 2003.
- [61] P. Martin, R. M. Murray, P. Rouchon, Flat systems, equivalence and trajectory generation, Tech. rep., CDS, California Institute of Technology (2003).
- [62] R. M. Murray, J. Hauser, A. Jadbabaie, M. B. Milam, N. Petit, W. B. Dunbar, R. Franz, Online control customization via optimization-based control. In T. Samad and G. Balas, Editors, *Software-Enabled Control: Information Technology for Dynamical Systems*, IEEE Press, 2003.
- [63] P. Martin, Contribution a l'étude des systemes differentiellement plats, Ph.D. thesis, Ecole des Mines de Paris (1992).
- [64] P. Martin, Aircraft control using flatness, in: *Proc. CESA Lille*, 1996.
- [65] J. Hauser, R. Hindman, Aggressive flight maneuvers, in: *IEEE Conf. on Decision and Control*, 1997.
- [66] F. Cazaurang, R. Bergeon, L. Lavigne, Modelling of longitudinal disturbed aircraft model by flatness approach, in: *AIAA Guidance Navigation and Control Conf.*, 2003.



- [67] W. C. Lu, L. Duan, F. B. Hsiao, F. M. Camino, Neural guidance control for aircraft based on differential flatness, *AIAA J. of Guidance, Control, and Dynamics* 31 (4) (2008) 892–898.
- [68] M. van Nieuwstadt, R. M. Murray, Outer flatness: Trajectory generation for a model helicopter, in: *Europ. Control Conf.*, 1997.
- [69] T. J. Koo, S. Sastry, Differential flatness based full authority helicopter control design, in: *IEEE Conf. on Decision and Control*, 1999.
- [70] I. D. Cowling, O. A. Yakimenko, J. F. Whidborne, A. K. Cook, A prototype of an autonomous controller for a quadrotor uav, in: *Europ. Control Conf.*, 2007.
- [71] D. Mellinger, V. Kumar, Minimum snap trajectory generation and control for quadrotors, in: *International Conf. on Robotics and Automation*, 2011.
- [72] S. Formentin, M. Lovera, Flatness-based control of a quadrotor helicopter via feedforward linearization, in: *IEEE Conf. on Decision and Control*, 2011.
- [73] A. Chamseddine, Z. Youmin, C. A. Rabbath, C. Join, D. Theilliol, Flatness-based trajectory planning/replanning for a quadrotor unmanned aerial vehicle, *IEEE Trans. on Aerospace and Electronic Systems* 48 (4) (2012) 2832–2848.
- [74] D. Henrion, J. B. Lasserre, Lmis for constrained polynomial interpolation with application in trajectory planning, *Systems & Control Letters* 55 (2006) 473–477.
- [75] M. B. Milam, K. Mushambi, R. M. Murray, A new computational approach to real-time trajectory generation for constrained mechanical systems, in: *IEEE Conf. on Decision and Control*, 2000.
- [76] R. Dai, B-splines based optimal control solution, in: *AIAA Guidance, Navigation and Control Conf.*, 2010.
- [77] F. Suryawan, J. A. D. Dona, M. M. Seron, Flatness-based minimum-time trajectory generation for constrained linear systems using b-splines, in: *IFAC World Congress*, 2011.

- [78] I. M. Ross, F. Fahroo, Pseudospectral methods for optimal motion planning of differentially flat systems, *IEEE Trans. Autom. Control* 49 (8) (2004) 1410–1413.
- [79] D. Desiderio, M. Lovera, Flatness-based guidance for planetary landing, in: *Am. Control Conf.*, 2010.
- [80] D. Bertsekas, *Nonlinear Programming - Second Edition*, Athena Scientific, Belmont, MA, 1999.
- [81] J. Nocedal, S. Wright, *Numerical Optimization*, Springer, NY, 2000.
- [82] R. J. Vanderbei, D. F. Shanno, An interior-point algorithm for nonconvex nonlinear programming, *Computational Optimization and Applications* 13 (1999) 231–252.
- [83] R. H. Byrd, M. E. Hribar, J. Nocedal, An interior point algorithm for large-scale nonlinear programming, *SIAM J. on Control and Optimization* 9 (4) (1999) 877–900.
- [84] L. T. Biegler, O. Ghattas, M. Heinkenschloss, B. van Bloemen Waanders, *Large-Scale PDE-Constrained Optimization*, Springer, Berlin, 2003.
- [85] R. H. Byrd, J. Nocedal, R. A. Waltz, *Knitro: An integrated package for nonlinear optimization*, *Large-Scale Nonlinear Optimization*, Springer-Verlag (2006) 35–59.
- [86] S. Taamallah, X. Bombois, P. M. J. Van den Hof, Optimal control for power-off landing of a small-scale helicopter a pseudospectral approach, in: *Am. Control Conf.*, 2012.
- [87] M. D. Ardema, N. Rajan, Separation of time scales in aircraft trajectory optimization, *AIAA J. of Guidance, Control, and Dynamics* 8 (2) (1985) 275–278.
- [88] S. Skogestad, I. Postlethwaite, *Multivariable Feedback Control: Analysis and Design*, 2nd Ed., Wiley-Interscience, Great Britain, 2005.

- [89] J. C. Doyle, Structured uncertainty in control system design, in: IEEE Conf. on Decision and Control, 1985.
- [90] K. Zhou, J. C. Doyle, K. Glover, Robust and Optimal Control, Prentice Hall, New Jersey, 1996.
- [91] A. A. G. Macintosh, Trajectory tracking control for a small-scale helicopter during autorotation, Tech. rep., Master Thesis, Delft University of Technology (2014).
- [92] <http://gemiddeldgezien.nl/meer-gemiddelden/176-gemiddelde-windkracht-nederland>.
- [93] Anonymous, Flying qualities of piloted airplanes, Tech. Rep. MIL-F-8785C, United States DoD (1980).
- [94] G. J. Balas, J. C. Doyle, K. Glover, A. K. Packard, R. S. Smith,  $\mu$  Analysis and Synthesis Toolbox: User's Guide, The MathWorks Inc., 1991.
- [95] K. Glover, All optimal hankel-norm approximations of linear multivariable systems and their  $\mathcal{L}_\infty$ -error bounds, Int. J. of Control 39 (6) (1984) 1115–1193.
- [96] A. Varga, A. Hansson, G. P. (Eds.), Optimization Based Clearance of Flight Control Laws - A Civil Aircraft Application, Springer, Lecture Notes in Control and Information Sciences, 2012.
- [97] J. L. Boiffier, The Dynamics of Flight The Equations, John Wiley & Sons, Chichester, England, 1998.



**NLR**

Anthony Fokkerweg 2

1059 CM Amsterdam, The Netherlands

p) +31 88 511 3113 f) +31 88 511 3210

e) [info@nlr.nl](mailto:info@nlr.nl) i) [www.nlr.nl](http://www.nlr.nl)